

Electronic Supplementary Information (ESI) for

Enantiopure 2-(2-ethylhexyl)dinaphtho[2,3-*b*:2',3'-*f*]thieno[3,2-*b*]thiophenes: synthesis, single crystal structure and surprising lack of influence of stereoisomerism on thin-film structure and electronic properties

Kenta Sumitomo^a, Yuta Sudo^a, Kiseki Kanazawa^{a,b}, Kohsuke Kawabata^{a,b}, Kazuo Takimiya^{a,b,c*}

^a Department of Chemistry, Graduate School of Science, Tohoku University, 6-3 Aoba, Aramaki, Aoba-ku, Sendai, Miyagi 980-8578, Japan

^b RIKEN Center for Emergent Matter Science (CEMS), 2-1 Hirosawa, Wako, Saitama 351-0198, Japan

^c Advanced Institute for Materials Research, Tohoku University (WPI-AIMR), 2-1-1 Katahira, Aoba-ku, Sendai, Miyagi 980-8577, Japan

Contents

1. Materials and Method	S2
2. OFET device fabrication and evaluation	S2–S3
3. Chiral resolution of 2-ethylhexanoic acid	S3–S5
4. Synthesis	S6–S12
5. X-ray structural analysis	S13
6. Optical microscope images of EH-DNTTs	S14–S15
7. Packing structure of parent DNTT	S15
8. Solubility evaluation of EH-DNTTs by ¹H NMR	S16
9. POM images of EH-DNTTs thin films	S17
10. AFM images of EH-DNTTs thin films	S18–S19
11. UV-vis absorption spectra of EH-DNTTs thin films	S20
12. Simulated powder pattern of <i>S</i>-EH-DNTT	S20
13. Optimized molecular structures of EH-DNTT with different conformations	S20
14. Partitioned E_{int}s calculated by F-SAPT	S21–S22
15. XRD curves of EH-BTBTs spin-coated thin films	S23
16. NMR spectra	S24–S37
17. References	S38

1. Materials and Method

All chemicals and solvents are of reagent grade unless otherwise indicated. Tetrahydrofuran (THF) and ether were purified with a Glass Contour solvent purification system prior to use. Racemic 2-ethylhexanoic acid (99.0% ee), (*R*)- and (*S*)-1-phenylethylamine (>99% ee) were purchased from TCI Chemicals. 2-Bromodinanaphtho[2,3-*b*:2',3'-*f*]thieno[3,2-*b*]thiophene (**Br-DNTT**)^{S1}, ethyl 2-bromobenzoate^{S2}, and 2-bromo-[1]benzothieno[3,2-*b*][1]benzothiophene (**Br-BTBT**)^{S3} were synthesized according to literature. Dichloromethane (DCM), 1,2-dimethoxyethane (DME), and *N,N*-dimethylformamide (DMF) used as reaction solvents were distilled over calcium hydride. All the reactions were carried out under nitrogen atmosphere. NMR spectra were recorded on JEOL JNM-ECS400, Bruker Avance III 500. ¹H and ¹³C NMR chemical shifts are reported in ppm relative to the signal for tetramethylsilane (0.00 ppm) or the signals for residual chloroform (77.0 ppm for ¹³C) or 1,1,2,2-tetrachloroethane (6.00 ppm for ¹H and 74.0 ppm for ¹³C) as internal standards. High-resolution mass spectrometry was carried out with a JEOL JMS-T100GCV mass spectrometer. Elemental analyses were performed with a J-Science Lab JM10 CHN corder, and all values are reported as percentages. Melting points of *R*-, *S*-, and *rac*-EHDNTTs were determined as the peak temperature of differential scanning calorimetry (DSC) curves recorded with a Shimadzu DSC-60 Plus at a heating and cooling rate of 10 °C min⁻¹. Gas chromatography (GC) using flame ionization detection was performed on a Shimadzu GC-2014 equipped with a Zebron ZB-1MS GC capillary column (30 m x ID:0.25 mm x df: 0.25 μm) using nitrogen gas as the carrier gas. Chiral HPLC analyses were performed on a Shimadzu LC-2010A HT Liquid Chromatograph system equipped with an UV detector and a COSMOSIL CHIRAL 3A (φ4.6 x 250 mm) packed column as the chiral stationary phase. UV-vis absorption spectra were recorded on a Shimadzu UV-3600 plus spectrometer. The solubilities of *R*-EH-DNTT, *S*-EH-DNTT, and *rac*-EH-DNTT in deuterated chloroform were estimated from the ¹H NMR spectra of their saturated solutions. For the solubility measurements, 5.00-mM solution of 2-bromo-6-methoxynaphthalene as an external standard. For the estimation of solubilities, the peak areas of four protons at 5-, 7-, 12-, 14-positions of the DNTT core and two protons at 4- and 8-positions of 2-bromo-6-methoxynaphthalene relative to the residual solvent peak were compared. All the ¹H NMR measurements for the estimation of the solubility were carried out under identical conditions on the same day with the deuterated chloroform from the same bottle. The DFT calculations were performed at the B3LYP/6-311G* level by using a Gaussian 16 program package.^{S4} Intermolecular interaction energies (E_{int}) and partitioned interaction energies were calculated by the symmetry-adapted perturbation theory (SAPT) and functional-group SAPT (F-SAPT) methods, respectively, with jun-cc-pvdz level using the PSI4 program package.^{S5, 6} Intermolecular electronic coupling (transfer integral, t) in different molecular dimers extracted from the single-crystal structures were calculated with the Amsterdam Density Functional (ADF) program.

S7

2. OFET device fabrication and evaluation

Bottom-gate-top-contact OFET devices were fabricated on a heavily doped n⁺-Si(100) wafer with 200-nm-thickness thermally grown SiO₂ ($C_i = 17.3 \text{ nF cm}^{-2}$). The Si/SiO₂ substrates (10 x 7 mm)

S2

were ultrasonicated with water for 3 min thrice, and with acetone and isopropanol for 10 min, respectively, and rinsed in boiling isopropanol for 10 min, and then were subjected to UV-ozone treatment for 30 min. The cleaned substrates were placed in the closed container in the presence of several drops of octyltrimethoxysilane (OTS) and kept in an oven at 80 °C overnight, and then the substrates were rinsed with boiling isopropanol. **R-EH-DNTT**, **S-EH-DNTT**, and **rac-EH-DNTT** were spin-coated on the OTS-treated Si/SiO₂ substrates from hot chloroform (containing 1 vol% of benzene) solutions (2.5 g L⁻¹) at a spin-rate of 3000 rpm for 30 sec, during which five drops of the hot chloroform solution were dropped onto the spinning substrate at the rate of 2 drops/sec. On the top of the thin films, gold drain and source contact electrodes (thickness: 40 nm) with the channel length and width of 100 and 1500 μm, respectively, were vacuum-deposited through shadow masks.

Current-voltage characteristics of the OFET devices were measured at rt under ambient conditions with a Keithley 4200-SCS semiconductor parameter analyzer. Threshold voltages of the devices were estimated from the transfer plots by extrapolating the square root of the drain current (in the range of $V_g = -30 - -60$ V for vacuum-deposition-based devices and $-50 - -80$ V for spin-coat-based devices) to the horizontal axis. Field-effect hole mobilities were extracted from the square root of the drain current by using the following equation and averaging over the range of $V_g = -30 - -60$ V for vacuum-deposition-based devices and $-50 - -80$ V for spin-coat-based devices.

$$\mu = \frac{2L}{WC_i} \cdot \left(\frac{d\sqrt{|I_d|}}{dV_g} \right)^2$$

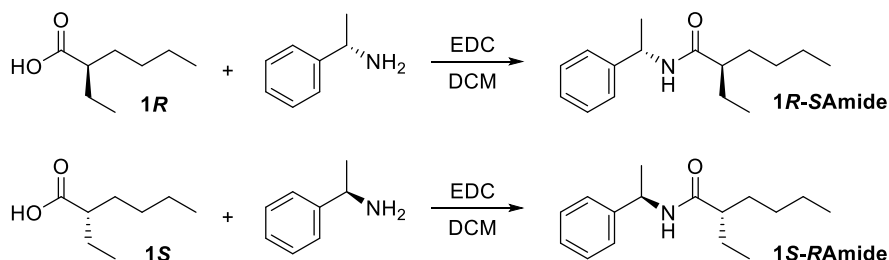
where, L and W are the channel length and width, respectively, and C_i is the capacitance of the gate insulator. The average hole mobility and threshold voltage were obtained from more than twelve devices for vacuum-deposited thin films, and from more than sixteen devices for spin-coated thin films.

3. Chiral resolution of 2-ethylhexanoic acid

The chiral resolution of racemic 2-ethylhexanoic acid was carried out by the formation and recrystallization of diastereomeric salts with (*R*)-1-phenylethylamine according to the reported procedure.^{S8} Recrystallization of the diastereomeric salts from hexane afforded a (*S*)-2-ethylhexanoate-enriched salt, which was further recrystallized from hexane four times to give (*R*)-1-phenylethylaminium (*S*)-2-ethylhexanoate. Acidification of the salts with 6 M hydrochloric acid followed by the extraction with hexane gave enantiopure (*S*)-2-ethylhexanoic acid (**1S**) (>97% ee estimated based on the diastereomeric ratio of an amide with (*R*)-1-phenylethylamine). Acidification of the filtrate solution of the first recrystallization for **1S** with 6 M hydrochloric acid gave *R*-enriched 2-ethylhexanoic acid, which was used for the formation and repeated recrystallization of the diastereomeric salts with (*S*)-1-phenylethylamine to give (*S*)-1-phenylethylaminium (*R*)-2-ethylhexanoate. Acidification of the salts with 6 M hydrochloric acid followed by the extraction with hexane gave enantiopure (*R*)-2-ethylhexanoic acid (**1R**) (>98% ee estimated based on the diastereomeric ratio of an amide with (*S*)-1-phenylethylamine).

The enantiomeric excesses of **1S** and **1R** were estimated based on the diastereomeric ratio of the diastereomeric amides, 2-ethyl-*N*-(1-phenylethyl)hexanamide, that were synthesized from **1R** with

(*S*)-1-phenylethylamine or **1S** with (*R*)-1-phenylethylamine via Steglich reaction in the presence of 1-(3-dimethylaminopropyl)-3-ethylcarbodiimide hydrochloride (EDC), in which almost no stereoselectivity for the reaction was observed. The diastereomeric ratio of the amides were determined by GC with a non-chiral stationary phase (Fig. S1).



To a mixture of **1R** (433 mg, 3.00 mmol) and (*S*)-1-phenylethylamine (545 mg, 4.60 mmol) in DCM (20 mL) was added EDC (866 mg, 4.50 mmol), and the mixture was stirred at room temperature for 3 h. The reaction mixture was washed with 1 M hydrochloric acid aqueous solution (30 mL x 5) and dried over magnesium sulfate. The crude product was purified by silica gel column chromatography (eluent: hexane/ethyl acetate = 3/1) to give **1R-SAmide** as a colorless solid (355 mg, 1.29 mmol, 43%). ¹H NMR (500 MHz, C₂D₂Cl₄) δ (ppm) 7.37–7.26 (m, 5H), 5.70 (d, 1H, J = 8.0 Hz), 5.13 (quintet, 1H, J = 7.1 Hz), 1.93–1.88 (m, 1H), 1.62–1.20 (m, 12H), 0.90 (t, 3H, J = 7.0 Hz), 0.84 (t, 3H, J = 7.3 Hz). ¹³C NMR (125 MHz, C₂D₂Cl₄) δ (ppm) 174.98, 143.57, 128.73, 127.32, 126.20, 49.70, 48.42, 32.56, 29.90, 26.15, 22.89, 22.01, 14.23, 12.33. HRMS (FD) m/z : [M]⁺ calcd for C₁₆H₂₅NO, 247.1936, found 247.1935.

The same procedure was applied to synthesize **1S-RAmide**. ¹H NMR (500 MHz, C₂D₂Cl₄) δ (ppm) 7.37–7.26 (m, 5H), 5.71 (d, 1H, J = 8.0 Hz), 5.13 (quintet, 1H, J = 7.1 Hz), 1.93–1.88 (m, 1H), 1.62–1.20 (m, 12H), 0.90 (t, 3H, J = 7.0 Hz), 0.84 (t, 3H, J = 7.3 Hz). ¹³C NMR (125 MHz, C₂D₂Cl₄) δ (ppm) 175.00, 143.56, 128.72, 127.32, 126.20, 49.70, 48.42, 32.56, 29.90, 26.15, 22.89, 22.01, 14.22, 12.33. HRMS (FD) m/z : [M]⁺ calcd for C₁₆H₂₅NO, 247.1936, found 247.1932.

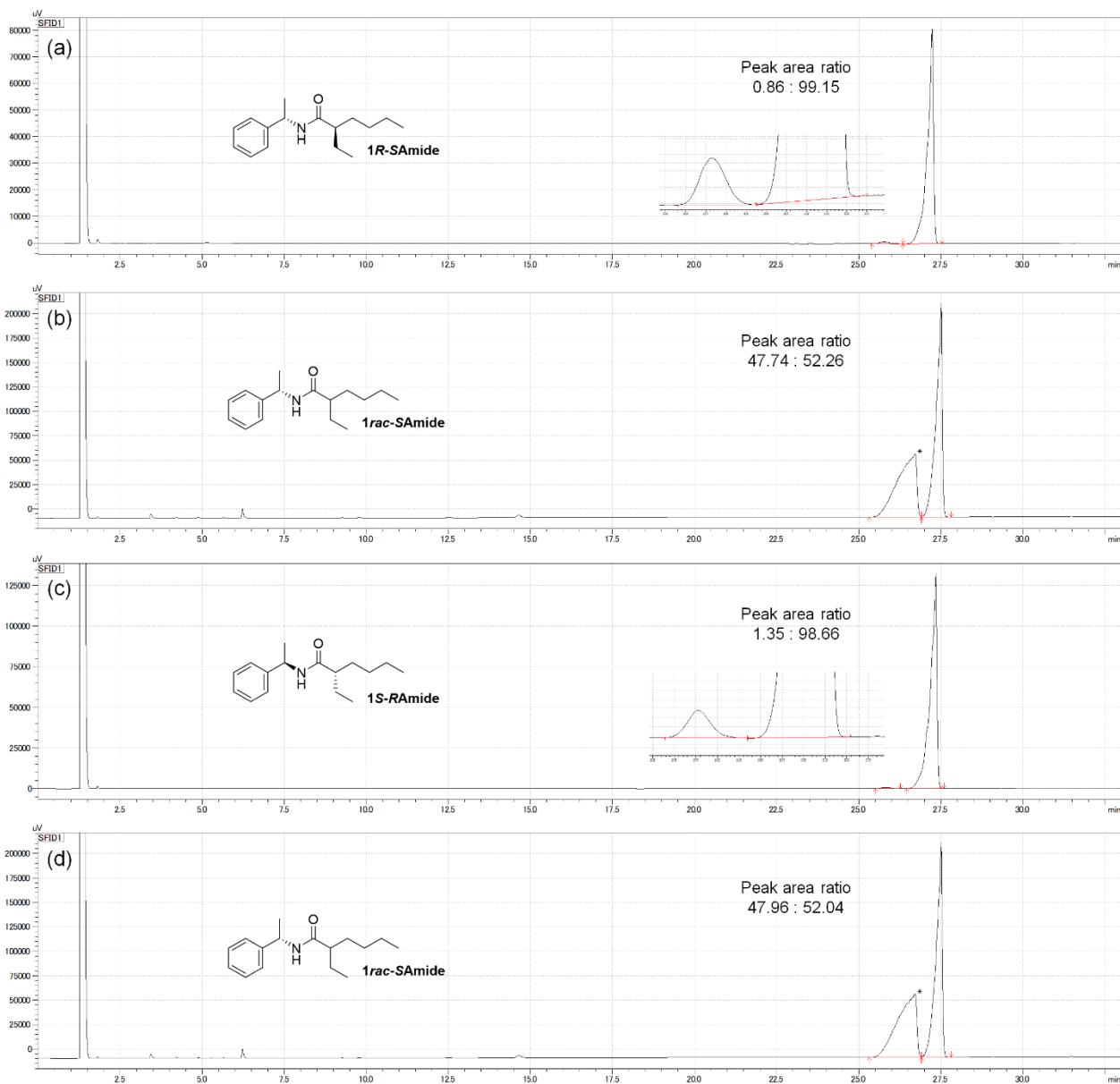
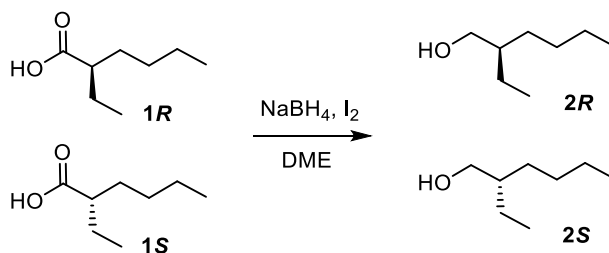


Fig. S1. GC charts for **1R-SAmide** (a), **1rac-SAmide** (b), **1S-RAmide** (c), and **1rac-SAmide** (d).

4. Synthesis

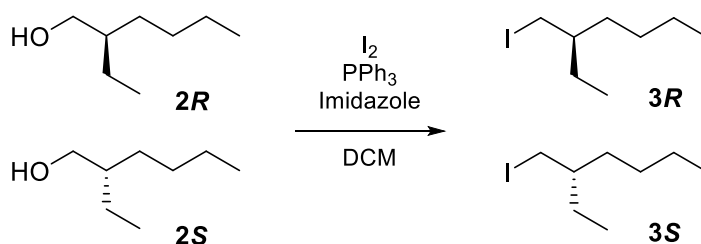
(*R*)- or (*S*)-2-Ethylhexanol (**2R** or **2S**)^{S9}



A solution of **1R** (23.7 mL, 21.6 g, 150 mmol) in DME (60 mL) was slowly added to a suspension of sodium borohydride (6.82 g, 180 mmol) in DME (60 mL) at room temperature. The mixture was stirred until evolution of gas ceases. After the solution was cooled to 0 °C, iodine (22.8 g, 90 mmol) in DME (60 mL) was added over 20 min. The solution was further stirred for 4 h at the same temperature. A solution of hydrochloric acid (5 M, 350 mL) was carefully added to the solution, and the organic layer was separated and washed successively with a solution of sodium hydroxide (6 M, 400 mL), a sodium hydroxide solution (1 M 200 mL x 2), a sodium thiosulfate aqueous solution (5%, 200 mL), and was dried over MgSO₄. Evaporation of the solvent gave crude colorless oil, which was purified by silica gel column chromatography eluted with DCM to give **2R** as a colorless liquid (17.3 g, 133 mmol, 89%). ¹H NMR (500 MHz, CDCl₃) δ (ppm) 3.55 (d, 2H, *J* = 5.0 Hz), 1.42–1.26 (m, 9H), 0.90 (t, 6H, *J* = 7.0 Hz). ¹³C NMR (125 MHz, CDCl₃) δ (ppm) 65.32, 41.97, 30.11, 29.11, 23.33, 23.08, 14.08, 11.09.

The same procedure was applied to synthesize **2S**. ¹H NMR (500 MHz, CDCl₃) δ (ppm) 3.55 (d, 2H, *J* = 5.0 Hz), 1.42–1.29 (m, 9H), 0.90 (t, 6H, *J* = 7.0 Hz). ¹³C NMR (125 MHz, CDCl₃) δ (ppm) 65.32, 41.97, 30.11, 29.11, 23.33, 23.08, 14.08, 11.09.

(*R*)- or (*S*)-2-Ethylhexyliodide (**3R** or **3S**)^{S10}

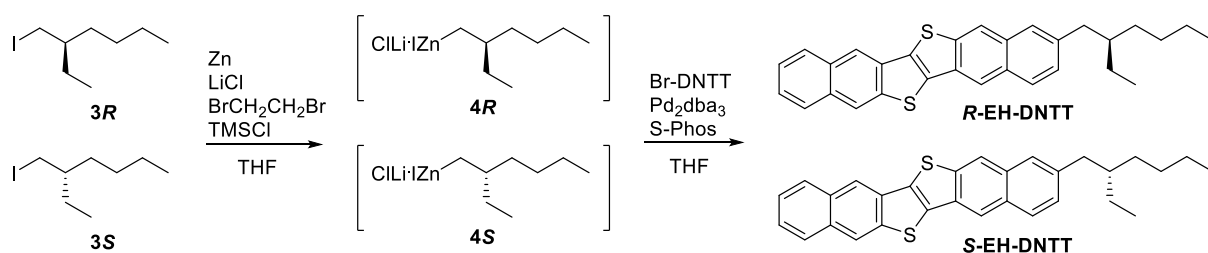


Into a solution of triphenylphosphine (9.44 g, 36.0 mmol) and imidazole (2.66 g, 39.0 mmol) in DCM (90 mL), iodine (9.14 g, 36.0 mmol) was added in portionwise at 0 °C. **2R** (3.42 g, 26.3 mmol) was added dropwise into the mixture, and the reaction mixture was stirred for 15 h at room temperature. A saturated aqueous solution of sodium hydrogen carbonate (60 mL) was added to the mixture, and the organic layer in the mixture was separated, washed subsequently with diluted hydrochloric acid (1 M, 60 mL x 3), and a sodium thiosulfate aqueous solution (5 wt%, 60 mL x 2), and was then dried (MgSO₄). Evaporation of the solvent gave a wet white solid, which was suspended in hexane (100 mL), and the insoluble portion was filtered off. The filtrate was concentrated under reduced pressure to give colorless oil, which was purified by silica gel column chromatography eluted with hexane to

give **3R** as a colorless liquid (5.60 g, 23.3 mmol, 89%). ¹H NMR (500 MHz, CDCl₃) δ 3.28 (m, 2H), 1.42–1.19 (m, 8H), 1.07 (septet, 1H, *J* = 5.7 Hz) 0.91 (t, 3H, *J* = 7.0 Hz), 0.87 (t, 3H *J* = 7.3 Hz). ¹³C NMR (125 MHz, CDCl₃) δ(ppm) 40.30, 33.69, 28.77, 27.03, 22.77, 16.19, 14.06, 10.85. HRMS (FD) *m/z*: [M]⁺ calcd for C₈H₁₇I, 240.0375, found 240.0372. Anal. Calcd for C₈H₁₇I: C, 40.02; H, 7.14. Found: C, 40.10; H, 7.38.

The same procedure was applied to synthesize **3S**. ¹H NMR (500 MHz, CDCl₃) δ 3.28 (m, 2H), 1.42–1.19 (m, 8H), 1.07 (septet, 1H, *J* = 5.7 Hz) 0.91 (t, 3H, *J* = 7.0 Hz), 0.87 (t, 3H *J* = 7.5 Hz). ¹³C NMR (125 MHz, CDCl₃) δ(ppm) 40.30, 33.68, 28.77, 27.03, 22.77, 16.18, 14.06, 10.85. HRMS (FD) *m/z*: [M]⁺ calcd for C₈H₁₇I, 240.0375, found 240.0373. Anal. Calcd for C₈H₁₇I: C, 40.02; H, 7.14. Found: C, 40.02; H, 7.12.

(*R*)- or (*S*)-2-(2-Ethylhexyl)dinaphtho[2,3-*b*:2',3'-*f*]thieno[3,2-*b*]thiophene (***R***- or ***S***-EH-DNTT)

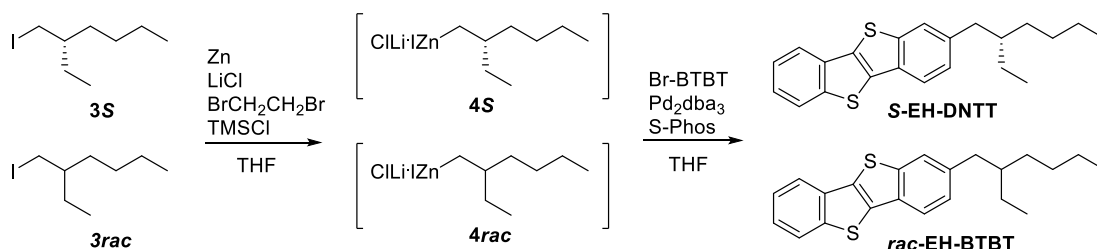


Lithium chloride (424 mg, 10.0 mmol) and zinc powder (785 mg, 12.0 mmol) were added in a 50 mL Schlenk tube and dried at 160 °C under vacuum for 15 min. After cooled to room temperature, THF (5.0 mL) and 1,2-dibromoethane (40 μL, 0.50 mmol) were added to the mixture, and the resulting mixture was refluxed for seconds, and then trimethylsilylchloride (10 μL, 0.10 mmol) was added. After cooled to room temperature, **3R** (2.40 g 10.0 mmol) was added to the mixture, and the resulting mixture was stirred at 60 °C for 36 h. The resulting (*R*)-2-ethylhexylzinc(II) iodide lithium chloride complex (**4R**) solution in THF (0.75 M determined by titillation with iodine) (5.6 mL, 4.2 mmol) was added to a mixture of BrDNTT (167 mg, 0.40 mmol), tris(dibenzylideneacetone)dipalladium(0) (Pd₂(dba)₃) (16 mg, 0.015 mmol), and dicyclohexyl(2',6'-dimethoxy[1,1'-biphenyl]-2-yl)phosphane (S-Phos) (25 mg, 0.060 mmol) in THF (15 mL), and the mixture was refluxed for 72 h. The mixture was diluted with DCM (200 mL) and passed through a silica gel column eluted with DCM. After the evaporation of the solvent, the yellow solid was washed by ultrasonication in methanol to afford **R**-EH-DNTT as a yellow solid (199 mg, 0.44 mmol, 73%). Analytical and device-grade sample was obtained by further purification by recrystallization from toluene and vacuum sublimation (1.0 Pa, 290 °C). **R**-EH-DNTT: ¹H NMR (CDCl₃, 500 MHz) δ 8.42 (s, 1H), 8.36 (s, 1H), 8.35 (s, 1H), 8.33 (s, 1H), 8.05–8.03 (m, 1H), 7.96–7.94 (m, 2H), 7.67 (s, 1H), 7.55–7.52 (m, 2H), 7.37 (dd, 1H, *J* = 8.5, 1.5 Hz), 2.79–2.71 (m, 2H), 1.72 (septet, 1H, *J* = 6.3 Hz), 1.39–1.26 (m, 8H), 0.92 (t, 3H, *J* = 7.5 Hz), 0.89 (t, 3H, *J* = 7.3 Hz). ¹³C NMR (100 MHz, C₂D₂Cl₄, 120 °C) δ(ppm) 141.05, 141.01, 140.05, 134.12, 133.43, 132.65, 131.99, 131.87, 131.66, 131.54, 130.15, 128.25, 128.23, 127.94, 127.32, 126.43, 125.91, 125.71, 122.42, 121.88, 119.94, 119.86, 41.12, 40.82, 32.98, 29.09, 26.14, 22.89, 13.80, 10.87. M.p. (*T*_{onset}^{DSC}): 333.4 °C. HRMS (FD) *m/z*: [M]⁺ calcd for C₃₀H₂₈S₂, 452.1632, found 452.1631. Anal. Calcd for C₃₀H₂₈S₂: C, 79.60; H, 6.23. Found: C, 79.60; H, 6.25.

The same procedure was applied to synthesize **S-EH-DNTT**. ^1H NMR (CDCl_3 , 500 MHz) δ 8.42 (s, 1H), 8.36 (s, 1H), 8.35 (s, 1H), 8.33 (s, 1H), 8.05–8.03 (m, 1H), 7.96–7.94 (m, 2H), 7.68 (s, 1H), 7.55–7.52 (m, 2H), 7.37 (dd, 1H, $J = 8.5, 1.5$ Hz), 2.79–2.71 (m, 2H), 1.72 (septet, 1H, $J = 6.3$ Hz), 1.39–1.25 (m, 8H), 0.92 (t, 3H, $J = 7.5$ Hz), 0.89 (t, 3H, $J = 7.3$ Hz). ^{13}C NMR (100 MHz, $\text{C}_2\text{D}_2\text{Cl}_4$, 120 °C) δ (ppm) 141.04, 141.02, 140.05, 134.12, 133.44, 132.65, 131.99, 131.87, 131.66, 131.54, 130.15, 128.26, 128.23, 127.94, 127.32, 126.43, 125.91, 125.71, 122.42, 121.88, 119.94, 119.86, 41.13, 40.83, 32.99, 29.09, 26.14, 22.90, 13.81, 10.88. M.p. ($T_{\text{onset}}^{\text{DSC}}$): 334.2 °C. HRMS (FD) m/z : $[\text{M}]^+$ calcd for $\text{C}_{30}\text{H}_{28}\text{S}_2$, 452.1632, found 452.1631. Anal. Calcd for $\text{C}_{30}\text{H}_{28}\text{S}_2$: C, 79.60; H, 6.23. Found: C, 79.60; H, 6.30.

rac-EH-DNTT were prepared by once dissolving **R**- and **S-EH-DNTT** (1:1 ratio) in chloroform and evaporating the solvent. M.p. ($T_{\text{onset}}^{\text{DSC}}$): 333.2 °C.

(*R*)- or racemic 2-(2-Ethylhexyl)benzo[*b*]benzo[4,5]thieno[2,3-*d*]thiophene (**S**- or **rac-EH-BTBT**)



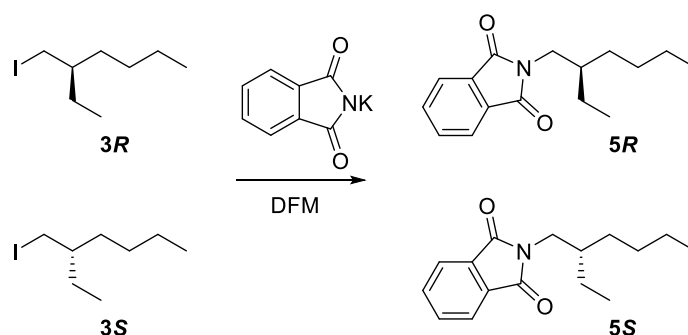
(*S*)-2-Ethylhexylzinc(II) iodide lithium chloride complex (**4S**) solution in THF (0.74 M determined by titillation with iodine) (4.5 mL, 3.3 mmol) was added to a mixture of **Br-BTBT** (319 mg, 1.0 mmol), tris(dibenzylideneacetone)dipalladium(0) ($\text{Pd}_2(\text{dba})_3$) (26 mg, 0.025 mmol), and dicyclohexyl(2',6'-dimethoxy[1,1'-biphenyl]-2-yl)phosphane (**S-Phos**) (41 mg, 0.10 mmol) in THF (8.5 mL), and the mixture was refluxed for 32 h. The reaction was quenched with 1M HCl aqueous solution (20 mL) and the mixture was extracted with *n*-hexane (100 mL), washed with water (100 mL x 3 times), and dried over magnesium sulfate. The crude product was purified by silica gel column chromatography eluted with *n*-hexane followed by recrystallization from ethanol to give **S-EH-BTBT** as colorless microcrystals (202 mg, 0.57 mmol, 57%). ^1H NMR (CDCl_3 , 400 MHz) δ 7.91 (ddd, 1H, $J = 8.0, 1.2, 0.8$ Hz), 7.86 (ddd, 1H, $J = 8.0, 1.2, 0.8$ Hz), 7.78 (dd, 1H, $J = 8.0, 0.4$ Hz), 7.69 (dd, 1H, $J = 1.4, 0.6$ Hz), 7.45 (ddd, 1H, $J = 8.0, 7.2, 1.2$ Hz), 7.38 (ddd, 1H, $J = 8.0, 7.2, 1.2$ Hz), 7.25 (dd, 1H, $J = 8.0, 1.6$ Hz), 2.70 (dd, $J = 13.6, 7.2$ Hz), 2.66 (dd, 1H, $J = 13.6, 7.2$ Hz), 1.66 (septet, 1H, $J = 6.2$ Hz), 1.37–1.24 (m, 8H), 0.92–0.86 (m, 6H). ^{13}C NMR (100 MHz, CDCl_3 , 20 °C) δ (ppm) 142.48, 142.08, 139.42, 133.41, 133.28, 132.58, 131.00, 126.59, 124.82, 124.71, 124.15, 124.01, 121.41, 121.11, 41.40, 40.32, 32.35, 28.87, 25.42, 23.05, 14.15, 10.82. M.p. ($T_{\text{onset}}^{\text{DSC}}$): 96.3 °C. HRMS (FD) m/z : $[\text{M}]^+$ calcd for $\text{C}_{22}\text{H}_{24}\text{S}_2$, 352.1319, found 352.1319. Anal. Calcd for $\text{C}_{22}\text{H}_{24}\text{S}_2$: C, 74.95; H, 6.86. Found: C, 74.91; H, 6.77.

The same procedure was applied to synthesize **rac-EH-BTBT** by using a racemic 2-

ethylhexylzinc(II) iodide lithium chloride complex (**4rac**) solution in THF. **rac-EH-BTBT** as colorless microcrystals (180 mg, 0.51 mmol, 51%). ¹H NMR (CDCl₃, 400 MHz) δ 7.91 (ddd, 1H, *J* = 8.0, 1.2, 0.8 Hz), 7.86 (ddd, 1H, *J* = 8.0, 1.2, 0.8 Hz), 7.78 (dd, 1H, *J* = 8.4, 0.4 Hz), 7.69 (dd, 1H, *J* = 1.2, 0.4 Hz), 7.45 (ddd, 1H, *J* = 8.0, 7.2, 1.2 Hz), 7.38 (ddd, 1H, *J* = 8.0, 7.2, 1.2 Hz), 7.25 (dd, 1H, *J* = 8.0, 1.6 Hz), 2.70 (dd, = 13.6, 7.2 Hz), 2.66 (dd, 1H, *J* = 13.6, 7.2 Hz), 1.66 (septet, 1H, *J* = 6.0 Hz), 1.37–1.24 (m, 8H), 0.92–0.87 (m, 6H). ¹³C NMR (100 MHz, CDCl₃, 20 °C) δ (ppm) 142.48, 142.08, 139.42, 133.41, 133.28, 132.58, 131.00, 126.59, 124.82, 124.71, 124.15, 124.01, 121.41, 121.11, 41.40, 40.32, 32.35, 28.87, 25.42, 23.05, 14.15, 10.82. M.p. (*T*_{onset}^{DSC}): 72.4 °C. HRMS (FD) *m/z*: [M]⁺ calcd for C₂₂H₂₄S₂, 352.1319, found 352.1318. Anal. Calcd for C₂₂H₂₄S₂: C, 74.95; H, 6.86. Found: C, 74.99; H, 6.83.

Because our chiral HPLC analyses for the determination of the enantiopurity of **3R** and **3S** were not successful, we carried out the derivatization of the iodide **3R** and **3S** to (*R*)- or (*S*)-2-(2-ethylhexyl)phthalimide (**5R** and **5S**), and then performed chiral HPLC analyses for **5R** and **5S** (Fig. S2).

(*R*)- or (*S*)-2-(2-Ethylhexyl)phthalimide (**5R** and **5S**)^{S11}



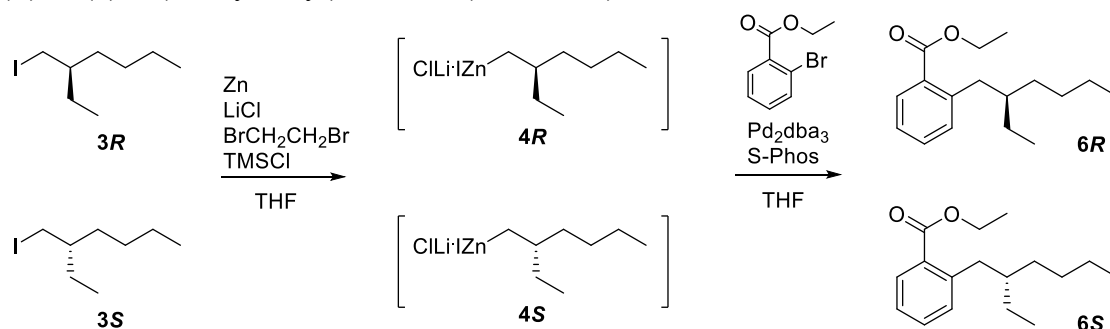
A solution of **3R** (480 mg, 2.00 mmol) and potassium phthalimide (407 mg, 2.20 mmol) in DMF (2.0 mL) was stirred at 60 °C for 24 h. The reaction mixture was poured into water (50 mL) and extracted with *n*-hexane (50 mL x 3). The combined organic layer was washed with water (150 mL x 3) and dried over magnesium sulfate. The crude product was purified by silica gel column chromatography (eluent: *n*-hexane/DCM = 1/1) to give **5R** as a colorless oil (491 mg, 1.89 mmol, 95%). ¹H NMR (500 MHz, CDCl₃) δ 7.86–7.82 (m, 2H), 7.73–7.69 (m, 2H), 3.58 (d, 2H, *J* = 7.5 Hz), 1.84 (septet, 1H, *J* = 6.2 Hz), 1.38–1.25(m, 8H), 0.92 (t, 3H, *J* = 7.5 Hz), 0.88 (t, 3H, *J* = 7.0 Hz). ¹³C NMR (125 MHz, CDCl₃) δ (ppm) 168.73, 133.81, 132.10, 123.13, 41.89, 38.29, 30.50, 28.49, 23.82, 22.97, 14.03, 10.39. Enantiomeric excess of **5R** was determined to be 98.5 %ee by chiral HPLC analysis (COSMOSIL CHiRAL 3A (φ4.6 x 250 mm), detection wavelength: 281 nm, eluent: *n*-hexane, flow rate: 1 mL min⁻¹, *t*_{major}: 10.5 min, *t*_{minor}: 11.8 min).

The same procedure was applied to synthesize **5S**. ¹H NMR (500 MHz, CDCl₃) δ 7.86–7.82 (m, 2H), 7.73–7.69 (m, 2H), 3.58 (d, 2H, *J* = 7.5 Hz), 1.84 (septet, 1H, *J* = 6.1 Hz), 1.40–1.25(m, 8H), 0.92 (t, 3H, *J* = 7.5 Hz), 0.88 (t, 3H, *J* = 7.0 Hz). ¹³C NMR (125 MHz, CDCl₃) δ (ppm) 168.73, 133.81, 132.10, 123.13, 41.88, 38.29, 30.50, 28.49, 23.82, 22.97, 14.03, 10.39. Enantiomeric excess of **5S**

was determined to be 99.1 %ee by chiral HPLC analysis (COSMOSIL CHiRAL 3A (φ4.6 x 250 mm), detection wavelength: 281 nm, eluent: *n*-hexane, flow rate: 1 mL min⁻¹, *t*_{major}: 11.8 min, *t*_{minor}: 10.6 min).

Our chiral HPLC analyses for the determination of the enantiopurity of *R*- and *S*-EH-DNTT were not successful. To confirm the retention of the stereochemistry of the ethylhexyl group through the last two synthetic steps for *R*- and *S*-EH-DNTT, namely, zinc insertion to **3R** and **3S** and subsequent palladium-catalyzed Negishi cross-coupling between the resulting organozinc species **4R** or **4S** and BrDNTT, we carried out a model Negishi cross-coupling reaction between **4R** or **4S** and ethyl 2-bromobenzoate to give ethyl (*R*) or (*S*)-2-(2-ethylhexyl)benzoate (**6R** and **6S**) under the exactly same condition used for the synthesis of *R*- and *S*-EH-DNTT, and then performed chiral HPLC analyses for **6R** and **6S** (Fig. S3).

Ethyl (*R*) or (*S*)-2-(2-ethylhexyl)benzoate (**6R** and **6S**)



The exactly same reaction condition for the synthesis of *R*-EH-DNTT, except the use of ethyl 2-bromobenzoate instead of BrDNTT, was applied for the synthesis of **6R**: ¹H NMR (CDCl₃, 500 MHz) δ 7.80 (dd, 1H, *J* = 8.0, 1.5 Hz), 7.38 (td, 1H, *J* = 7.5, 1.5 Hz), 7.25–7.20 (m, 2H), 4.35 (quartet, 2H, *J* = 7.2 Hz), 2.90 (d, 2H, *J* = 7.5 Hz) 1.57–1.51 (m, 1H), 1.39 (t, 3H, *J* = 7.30 Hz), 1.30–1.19 (m, 8H), 0.87–0.83 (m, 6H). ¹³C NMR (125 MHz, CDCl₃) δ (ppm) 168.27, 143.10, 131.70, 131.07, 130.81, 130.24, 125.57, 60.78, 40.89, 38.25, 32.24, 28.58, 25.35, 23.06, 14.30, 14.08, 10.60. HRMS (FD) *m/z*: [M]⁺ calcd for C₁₇H₂₆O₂, 262.1933, found 262.1931. Anal. Calcd for C₁₇H₂₆O₂: C, 77.82; H, 9.99. Found: C, 77.77; H, 10.06. Enantiomeric excess of **6R** was determined to be 98.5 %ee by chiral HPLC analysis (COSMOSIL CHiRAL 3A (φ4.6 x 250 mm), detection wavelength: 289 nm, eluent: *n*-hexane, flow rate: 1 mL min⁻¹, *t*_{major}: 7.3 min, *t*_{minor}: 7.0 min).

The same reaction condition for the synthesis of *S*-EH-DNTT, except the use of ethyl 2-bromobenzoate instead of BrDNTT, was applied for the synthesis of **6S**: ¹H NMR (CDCl₃, 500 MHz) δ 7.80 (dd, 1H, *J* = 8.0, 1.5 Hz), 7.38 (td, 1H, *J* = 7.5, 1.0 Hz), 7.25–7.20 (m, 2H), 4.35 (quartet, 2H, *J* = 7.2 Hz), 2.90 (d, 2H, *J* = 7.0 Hz) 1.57–1.51 (m, 1H), 1.39 (t, 3H, *J* = 7.3 Hz), 1.30–1.19 (m, 8H), 0.87–0.83 (m, 6H). ¹³C NMR (125 MHz, CDCl₃) δ (ppm) 168.27, 143.11, 131.70, 131.07, 130.82, 130.25, 125.57, 60.78, 40.89, 38.25, 32.25, 28.58, 25.35, 23.06, 14.31, 14.09, 10.60. HRMS (FD) *m/z*: [M]⁺ calcd for C₁₇H₂₆O₂, 262.1933, found 262.1031. Anal. Calcd for C₁₇H₂₆O₂: C, 77.82; H, 9.99. Found: C, 77.75; H, 9.91. Enantiomeric excess of **6S** could not be precisely determined because the minor peak was buried in the tail of the major peak (COSMOSIL CHiRAL 3A (φ4.6 x 250 mm),

detection wavelength: 289 nm, eluent: *n*-hexane, flow rate: 1 mL min⁻¹, t_{major} : 7.0 min, t_{minor} : not available).

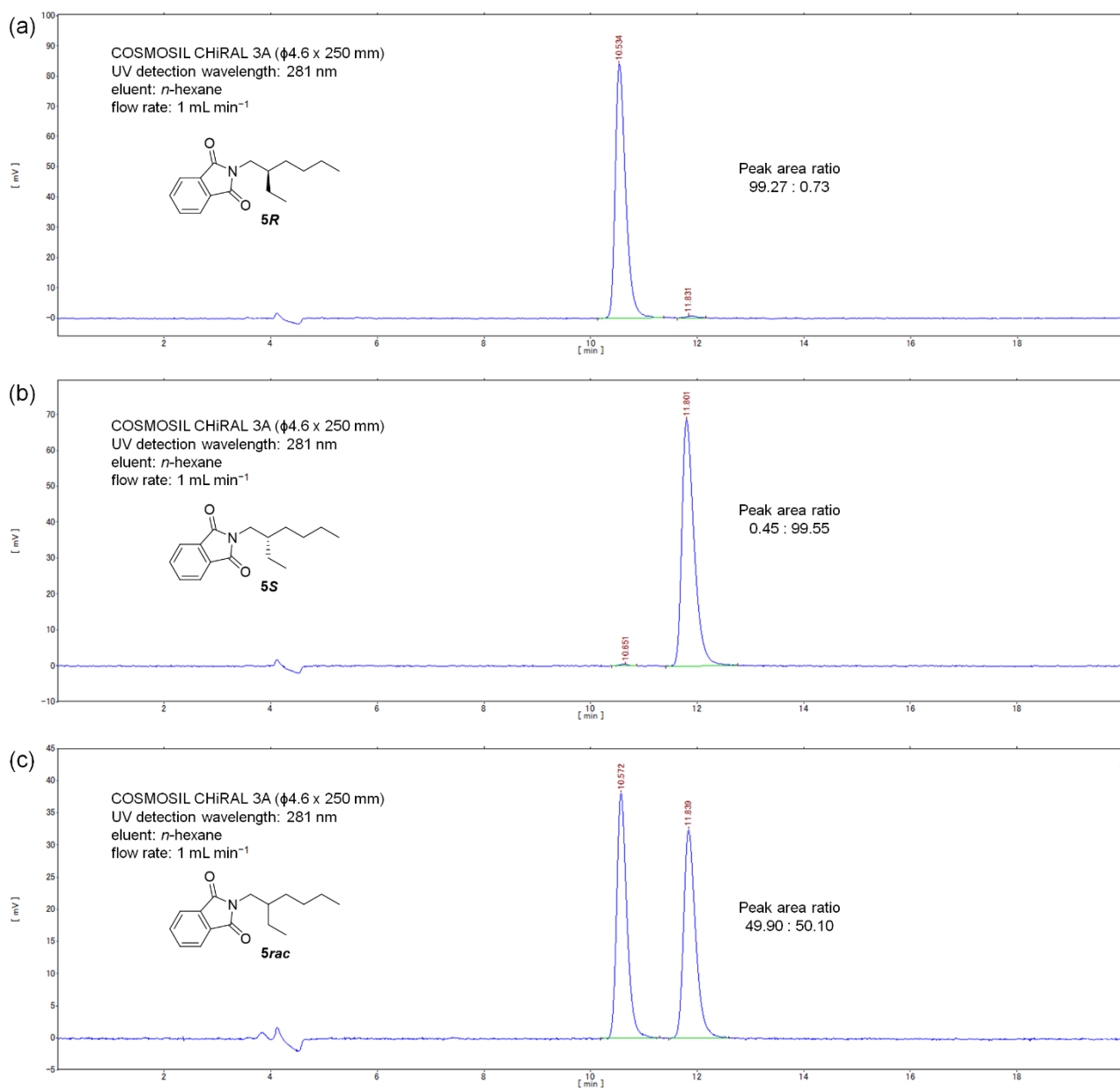


Fig. S2. Chiral HPLC charts of **5R** (a), **5S** (b), and their one-to-one racemic mixture (**5rac**) (c).

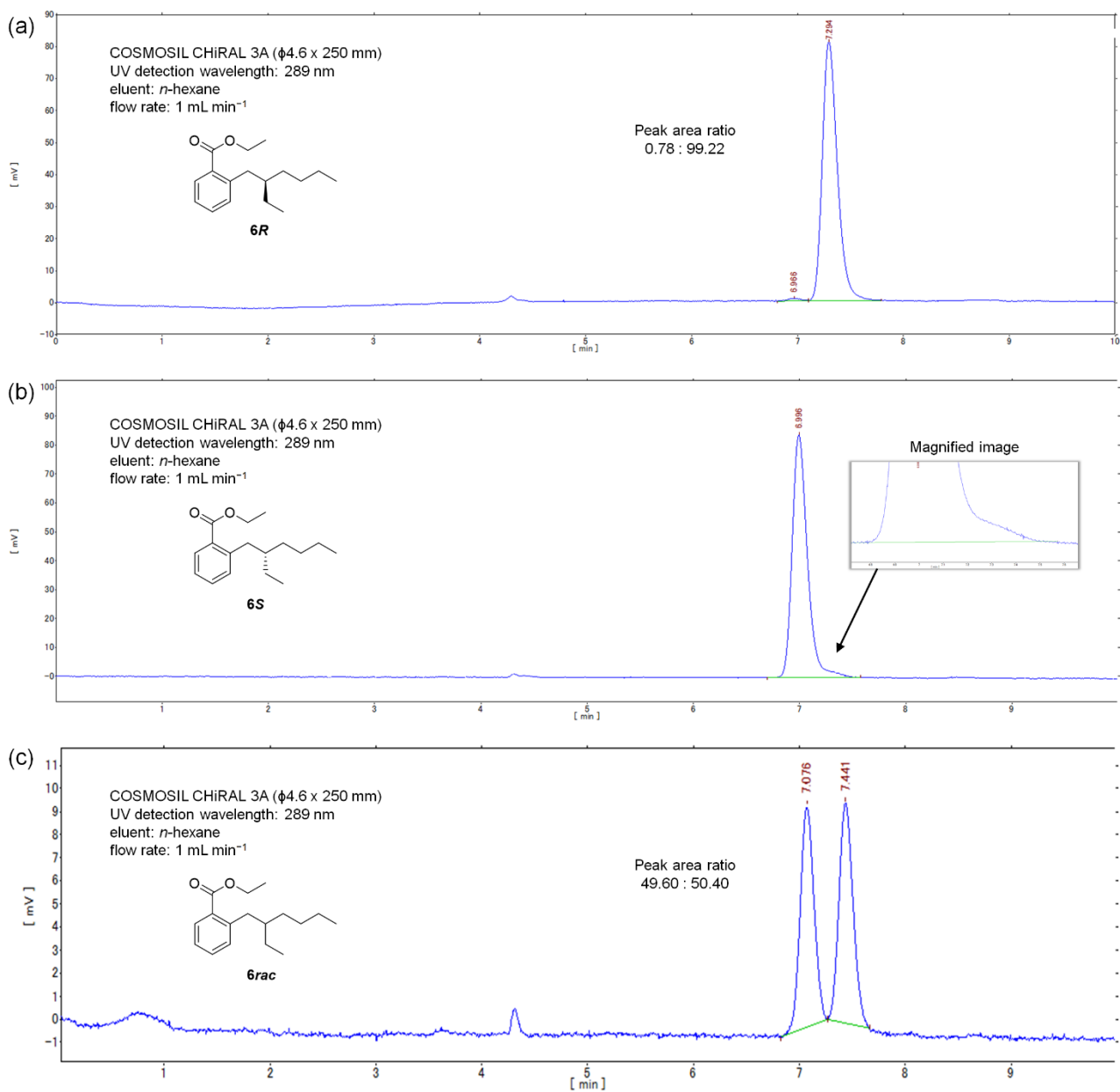


Fig. S3. Chiral HPLC charts of **6R** (a), **6S** (b), and their one-to-one racemic mixture (**6rac**) (c).

5. X-ray structural analysis

Single crystals of *R*- and *S*-EH-DNTT suitable for X-ray crystallographic analysis were grown by slow vapor diffusion of methanol into a 0.3 wt% solution of *R*- and *S*-EH-DNTT in toluene. Single-crystal X-ray analyses were carried out on a Rigaku Oxford Diffraction XtaLAB Synergy Custom DW system with a HyPix-6000HE detector (CuK α radiation, $\lambda = 1.5418 \text{ \AA}$, multilayer confocal optics). The structure was solved by the SHELXT program.^{S12} Non-hydrogen atoms were refined anisotropically.^{S13} All calculations were carried out by using the crystallographic software package Olex2 (ver. 1.3.0).^{S14} Crystallographic data of *R*-EH-DNTT: (deposited as CCDC-2096392). C₃₀H₂₈S₂, *triclinic*, *P1* (#1), $a = 6.60173(1)$, $b = 8.1041(2)$, $c = 24.3262(5) \text{ \AA}$, $\alpha = 98.542(2)$, $\beta = 94.452(2)$, $\gamma = 92.932(2)^\circ$, $V = 1167.20(4) \text{ \AA}^3$, $Z = 2$, $T = 100(2) \text{ K}$, $R = 0.0622$, $wR^2 = 0.1684$, GOF = 1.090, Flack parameter = 0.035(12). Crystallographic data of *S*-EH-DNTT: (deposited as CCDC-2092243). C₃₀H₂₈S₂, *triclinic*, *P1* (#1), $a = 6.0023(2)$, $b = 8.1084(2)$, $c = 24.3715(5) \text{ \AA}$, $\alpha = 98.319(2)$, $\beta = 94.455(2)$, $\gamma = 92.830(2)^\circ$, $V = 1167.90(5) \text{ \AA}^3$, $Z = 2$, $T = 100(2) \text{ K}$, $R = 0.0598$, $wR^2 = 0.1748$, GOF = 1.043, Flack parameter = 0.00(2).

6. Optical microscope images of EH-DNTTs

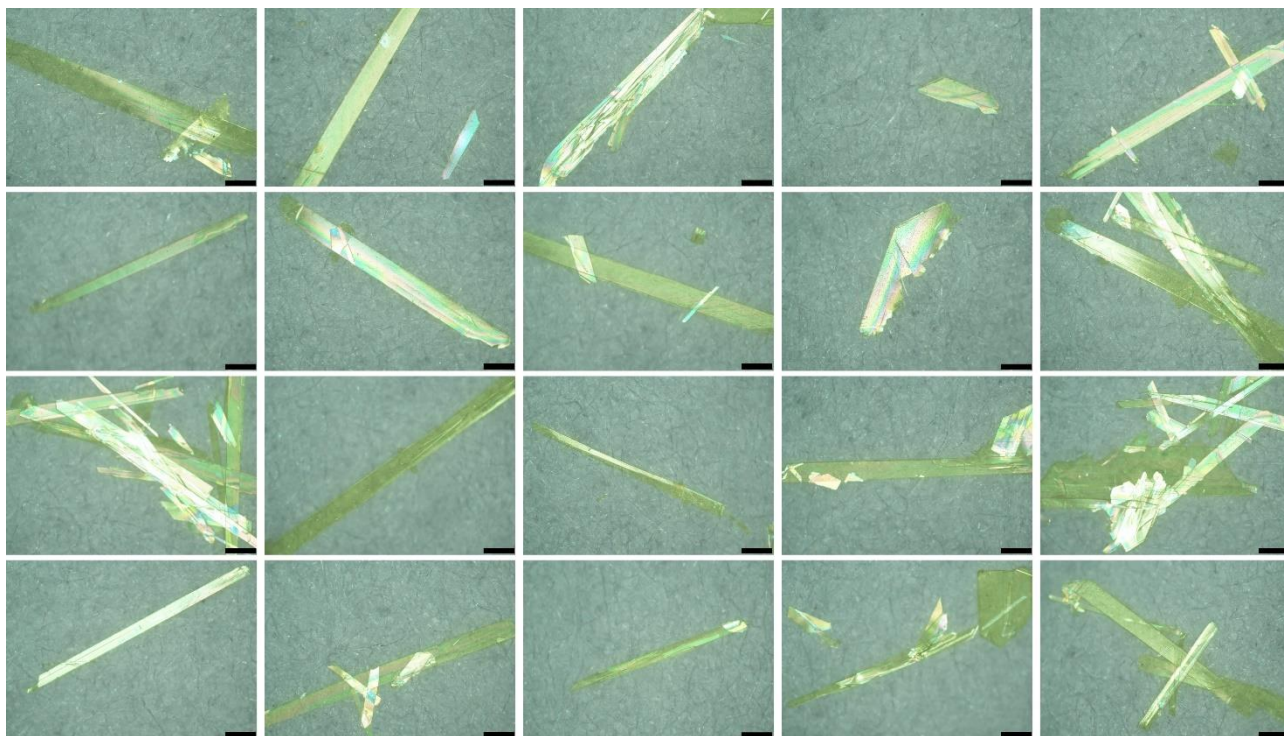


Fig. S4. Optical microscope images of crystalline **1R** recrystallized by slow vapor diffusion of methanol into a 0.3 wt% sample solution in toluene. Scale bars are 300 μm .

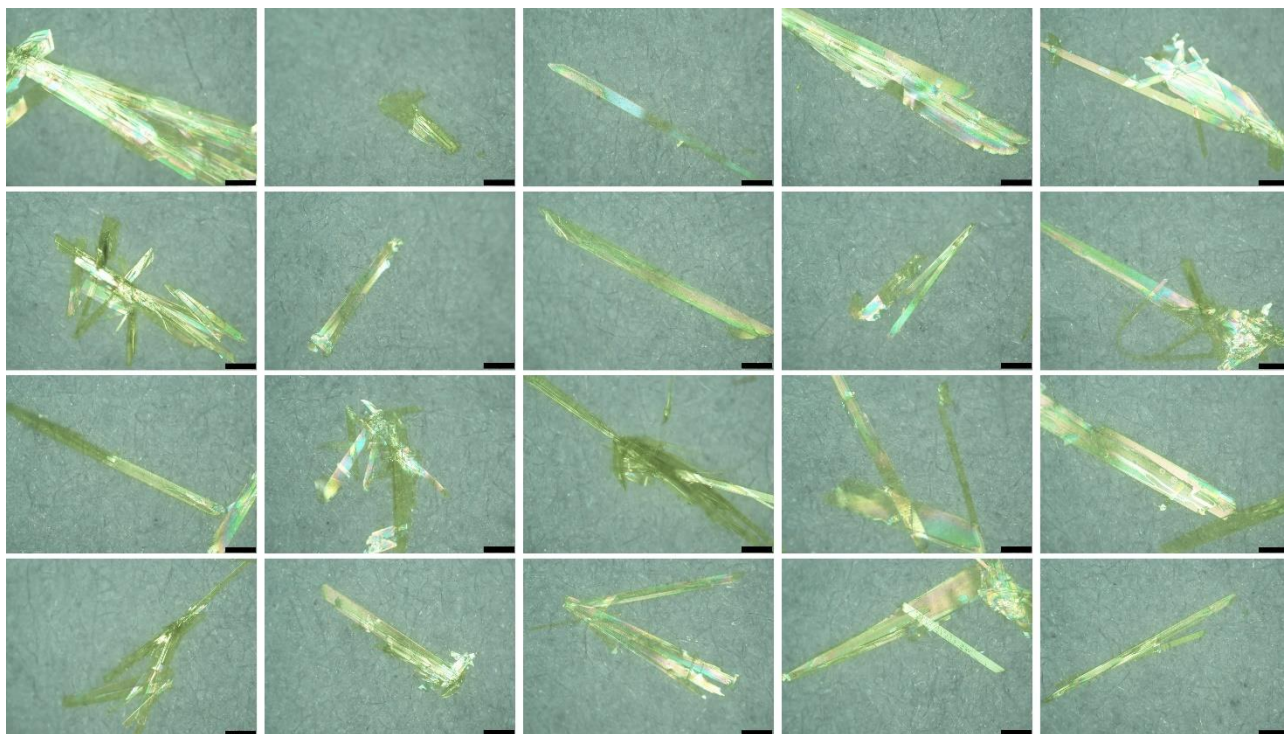


Fig. S5. Optical microscope images of crystalline **1S** recrystallized by slow vapor diffusion of methanol into a 0.3 wt% sample solution in toluene. Scale bars are 300 μm .

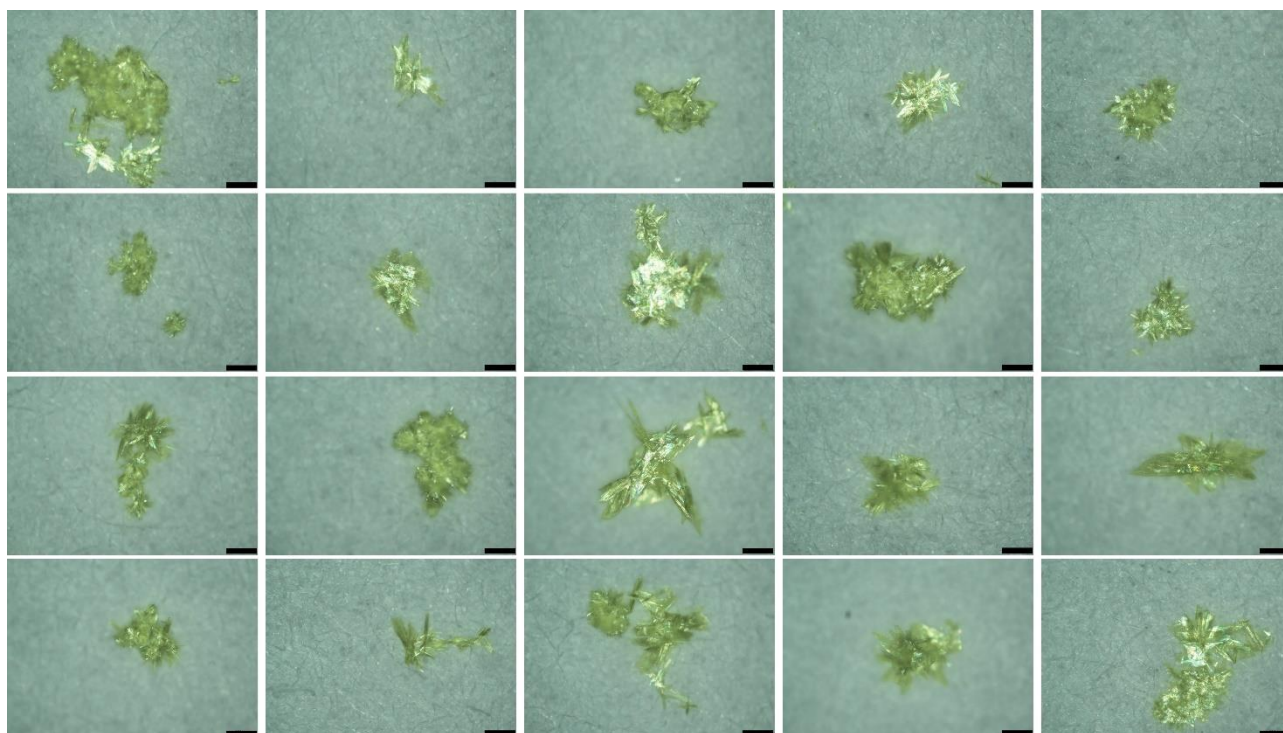


Fig. S6. Optical microscope images of crystalline **1rac** recrystallized by slow vapor diffusion of methanol into a 0.3 wt% sample solution in toluene. Scale bars are 300 μm .

7. Packing structure of parent DNTT

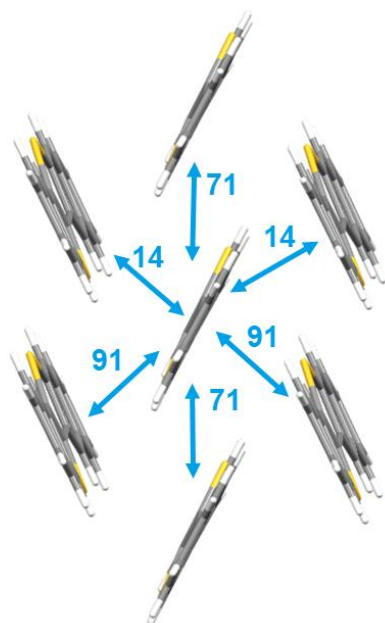


Fig. S7. Packing structure of parent DNTT and calculated transfer integrals (t_s , meV) of HOMO.

8. Solubility evaluation of EH-DNTTs by ^1H NMR

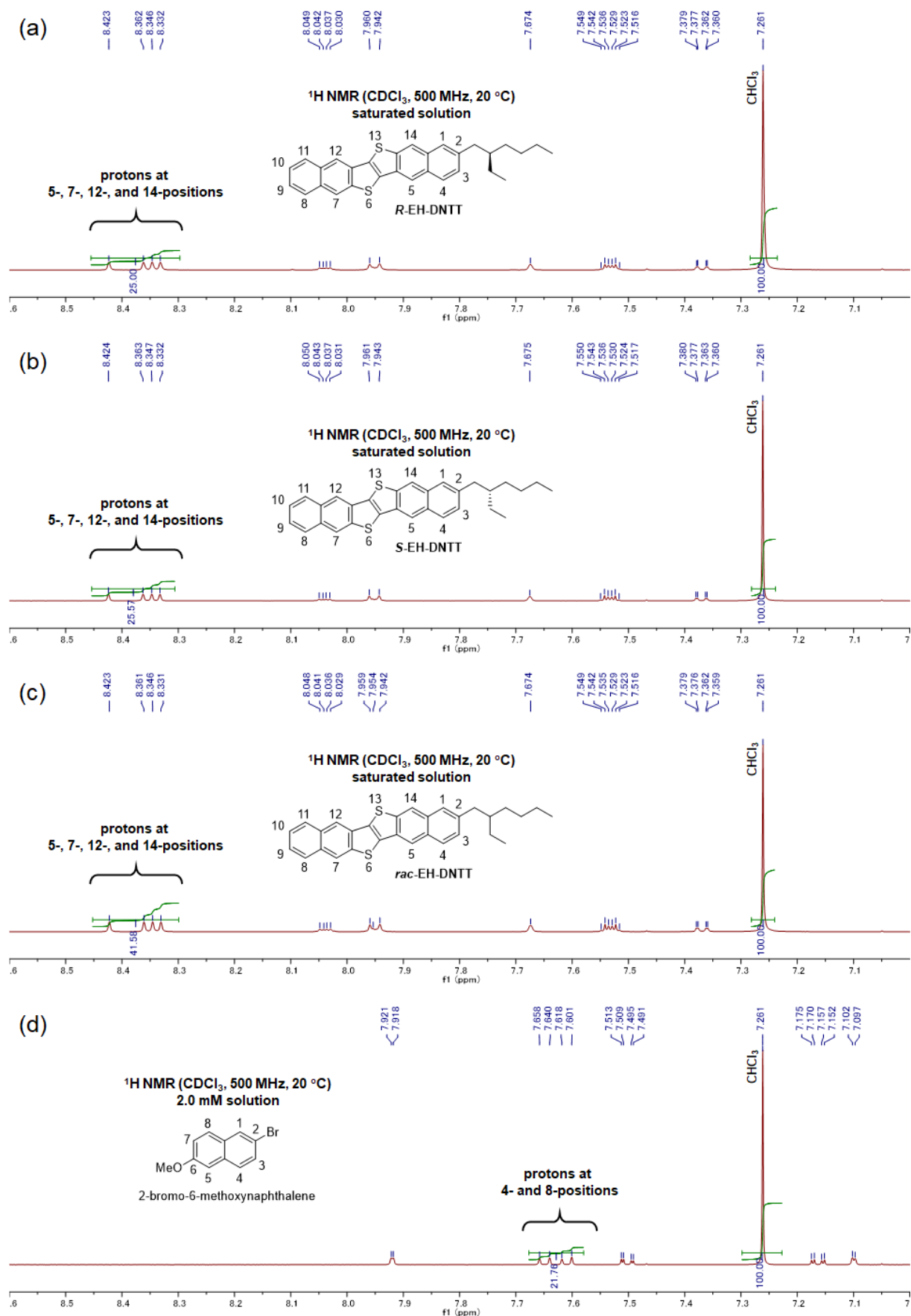


Fig. S8. ^1H NMR spectra of saturated solutions of *R*- (a), *S*- (b), and *rac*-EH-DNTT (c), and 2.0 mM 2-bromo-6-methoxynaphthalene solution in CDCl_3 at 20 °C.

9. POM images of EH-DNTTs thin films

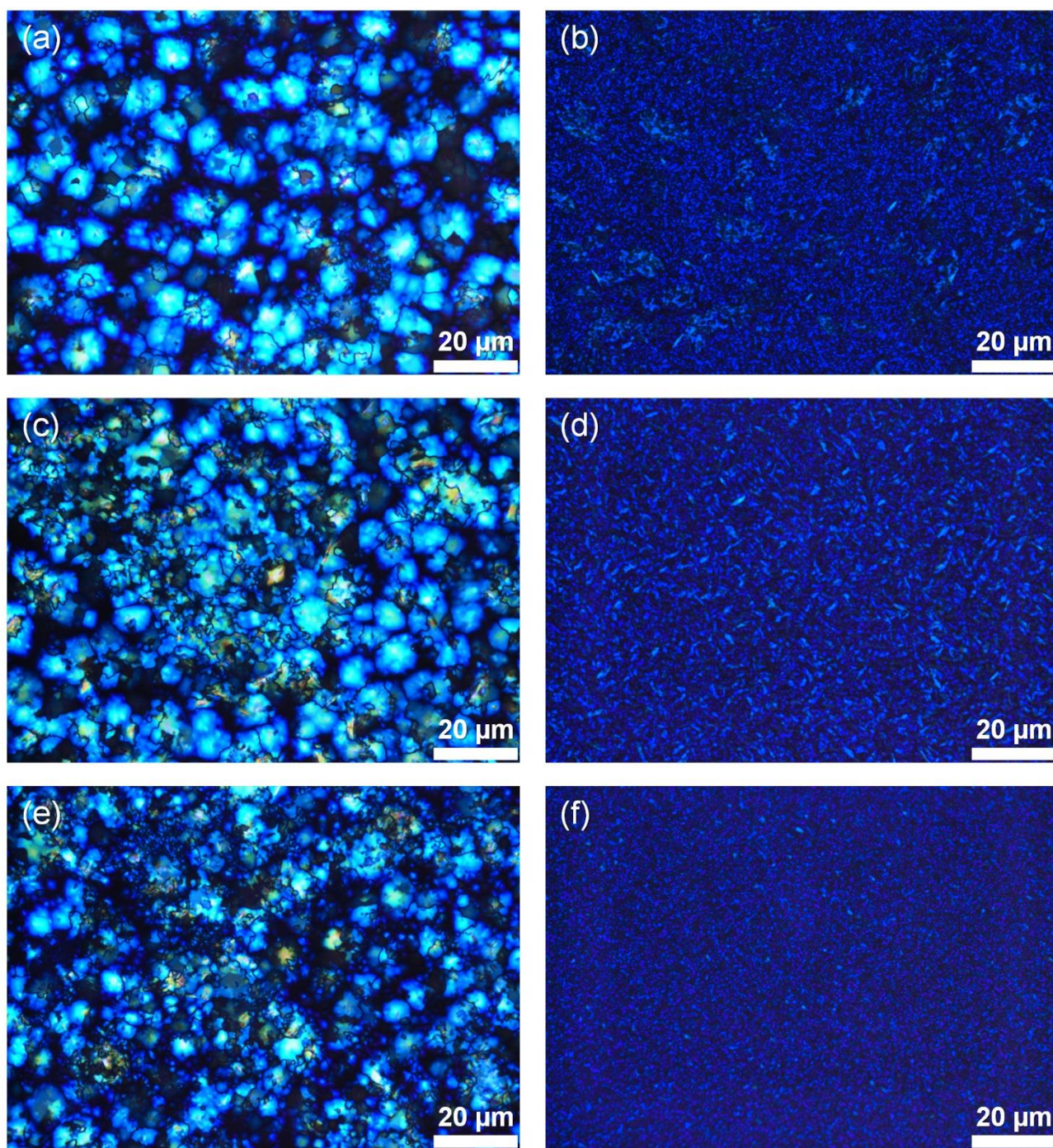


Fig. S9. POM images of spin-coated (a, c, e) and vacuum-deposited (b, d, f) thin films of *R*-EH-DNTT, *S*-EH-DNTT, and *rac*-EH-DNTT, respectively, on OTS-treated SiO₂/Si substrates.

10. AFM images of EH-DNTTs thin films

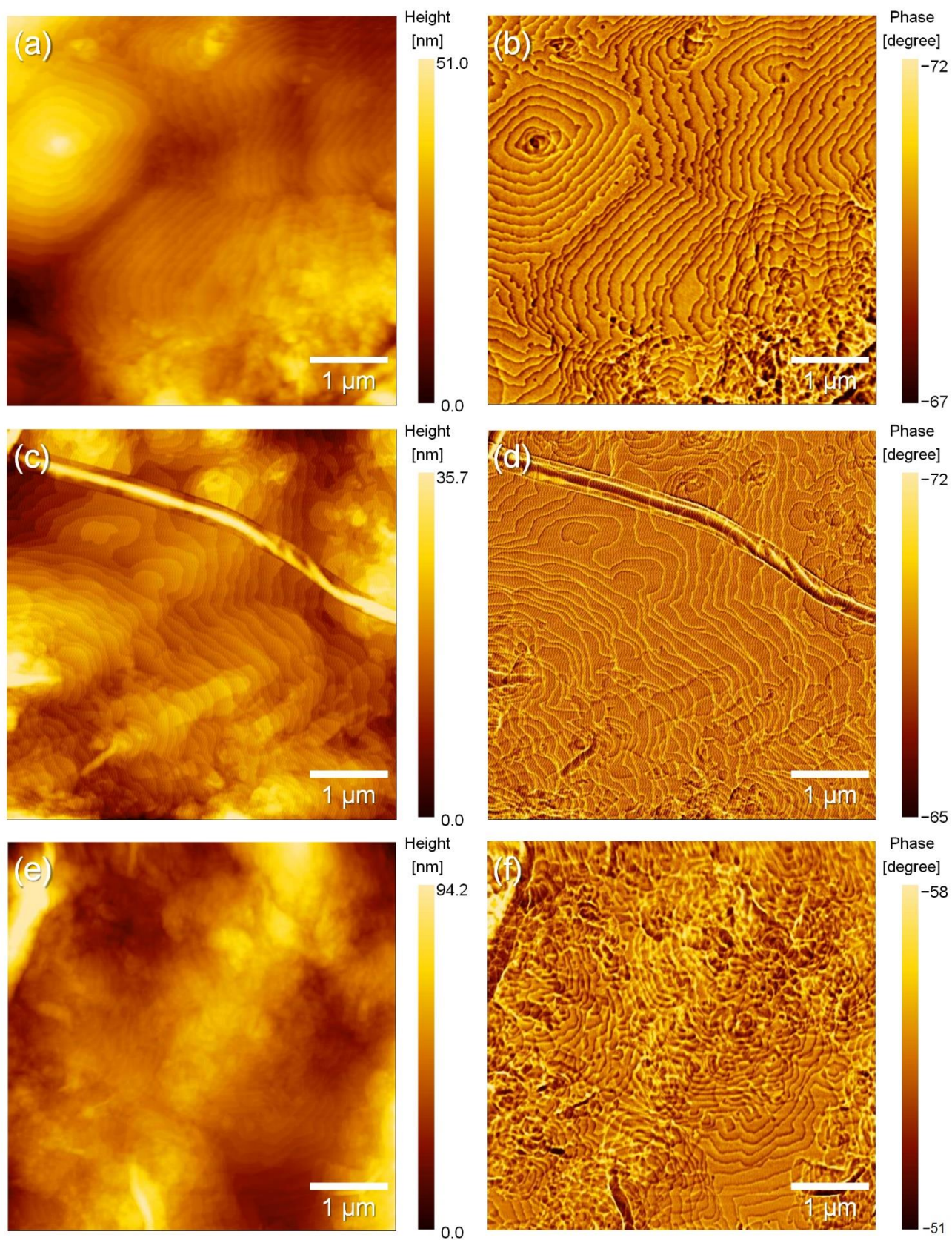


Fig. S10. AFM height and phase images of spin-coated thin films of *R*-EH-DNTT (a, b), *S*-EH-DNTT (c, d), and *rac*-EH-DNTT (e, f), respectively, on OTS-treated SiO₂/Si substrates.

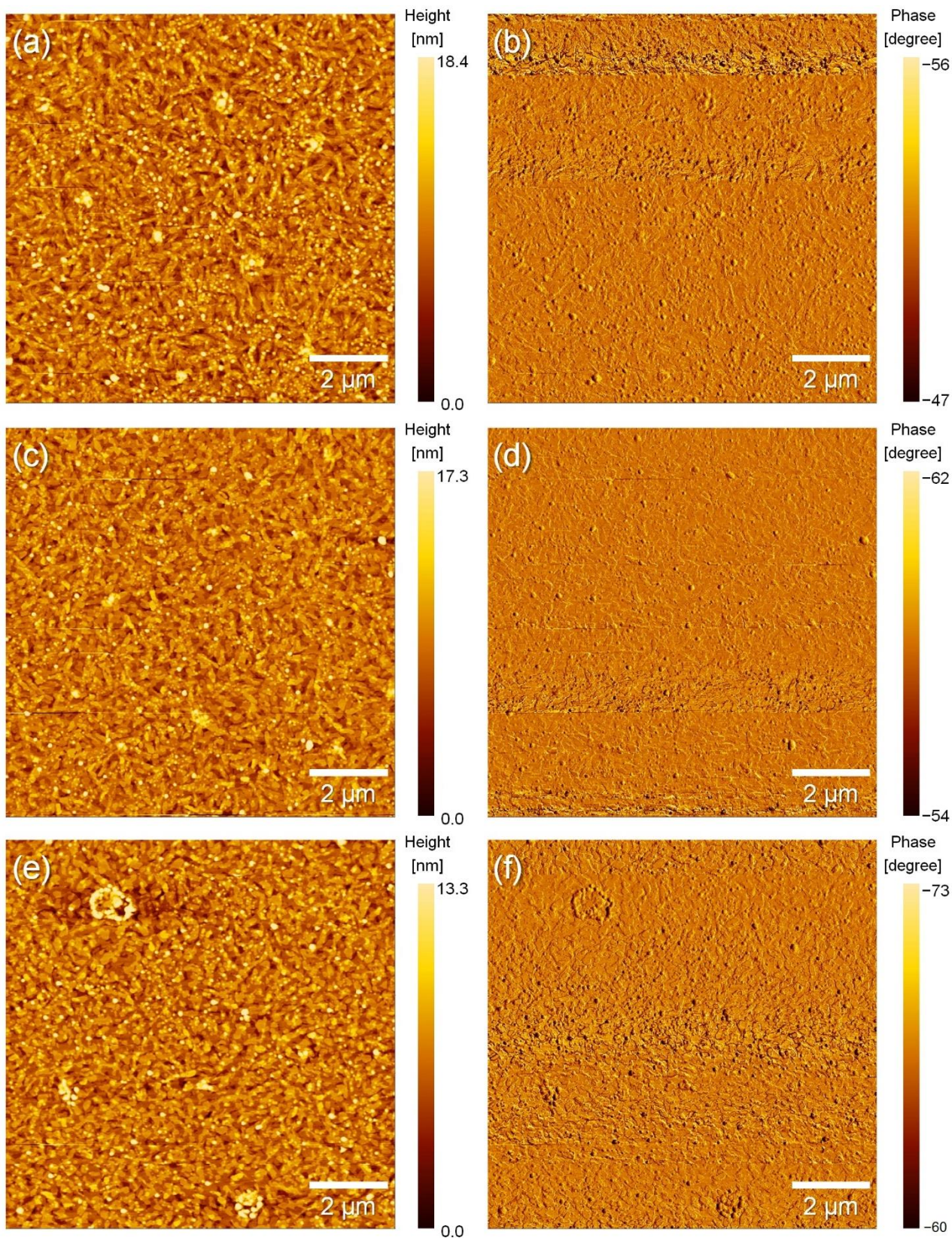


Fig. S11. AFM height and phase images of vacuum-deposited thin films of *R*-EH-DNTT (a, b), *S*-EH-DNTT (c, d), and *rac*-EH-DNTT (e, f), respectively, on OTS-treated SiO₂/Si substrates.

11. UV-vis absorption spectra of EH-DNTTs thin films

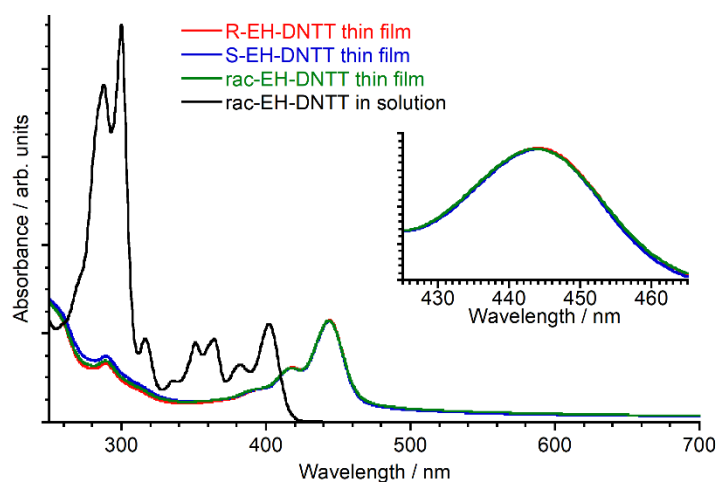


Fig. S12. UV-vis absorption spectra of vacuum-deposited thin films of *R*- (red), *S*- (blue), *rac*- (green) EH-DNTTs and *rac*-EH-DNTT in a chloroform solution (black). Inset is a magnified spectra around the absorption maxima of the thin films.

12. Simulated powder pattern of *S*-EH-DNTT

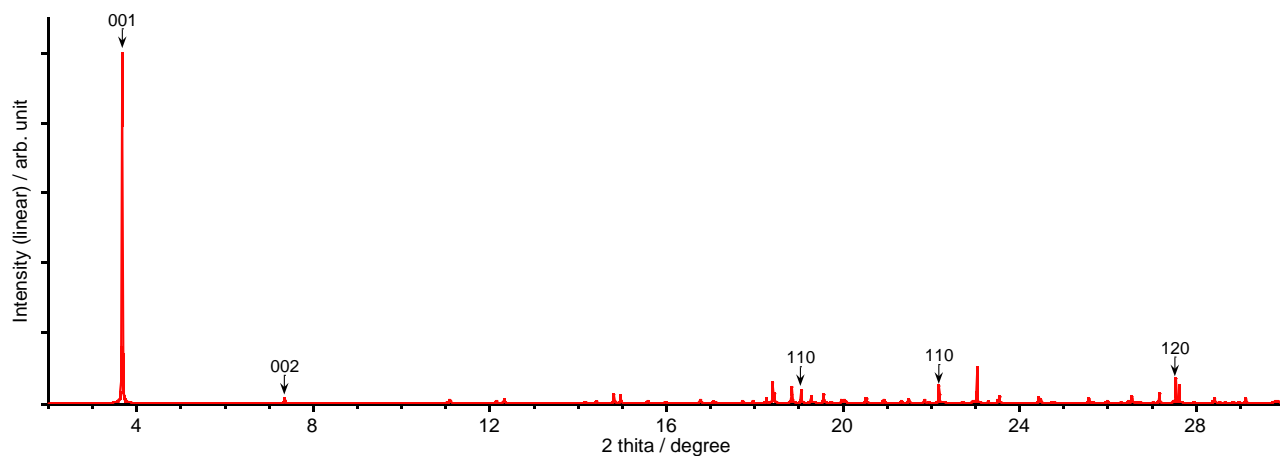


Fig. S13. A simulated x-ray powder diffraction pattern of *S*-EH-DNTT based on the single-crystal structure.

13. Optimized molecular structures of EH-DNTT with different conformations

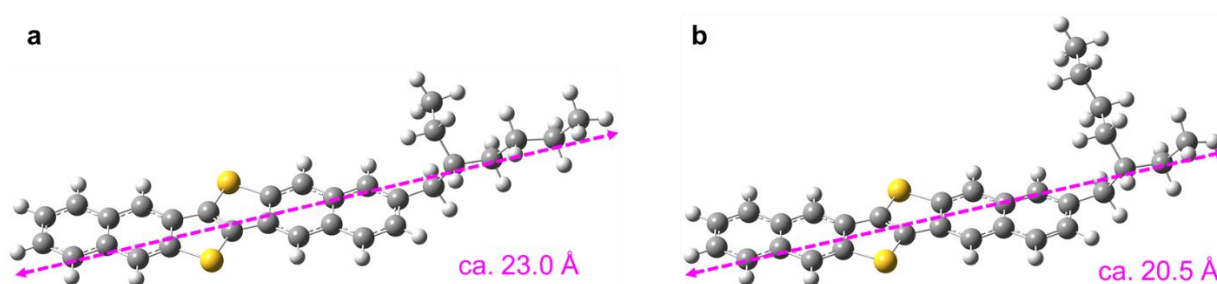
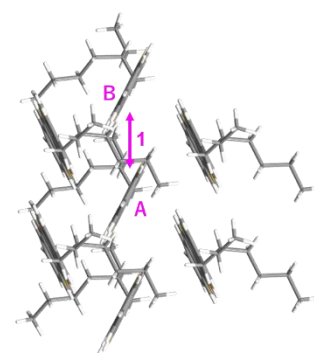


Fig. S14. Molecular lengths of EH-DNTT with the trunk-stretched (a) and the branch-stretched (b) structure.

14. Partitioned E_{ints} calculated by F-SAPT

Table S1. Partitioned intermolecular interaction energy ($E_{\text{ints}} / \text{kcal mol}^{-1}$) of the molecular pair #1^a.

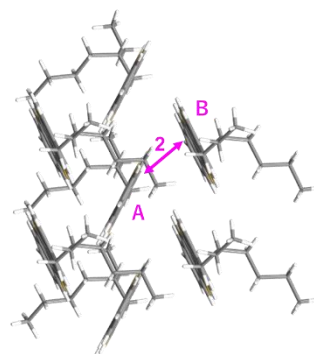
Mol A–Mol B	$E_{\text{elst}}^{\text{b}}$	$E_{\text{exch}}^{\text{b}}$	$E_{\text{indAB}}^{\text{b}}$	$E_{\text{indBA}}^{\text{b}}$	$E_{\text{disp}}^{\text{b}}$	$E_{\text{total}}^{\text{b}}$
DNTT–DNTT	-7.793	14.189	-0.841	-0.858	-15.463	-10.766
DNTT–EH	-0.263	0.001	-0.005	-0.016	-0.245	-0.528
EH–DNTT	-0.27	0.386	-0.079	0.02	-1.274	-1.217
EH–EH	0.024	0.482	-0.002	-0.006	-1.773	-1.275
total	-8.301	15.058	-0.927	-0.861	-18.756	-13.787
SAPT0 ^c	-8.300	15.059	-0.927	-0.861	-18.755	-13.785



^a Refer the inserted figure in Table 3 for the definition of the molecular pair. ^b E_{elst} : electrostatic interaction energy, E_{exch} : exchange interaction energy, E_{indAB} : induction interaction energy, E_{indBA} : induction interaction energy, E_{disp} : dispersion energy, E_{total} : the sum of each energetic terms. ^c E_{int} separately calculated by SAPT0.

Table S2. Partitioned intermolecular interaction energy ($E_{\text{ints}} / \text{kcal mol}^{-1}$) of the molecular pair #2^a.

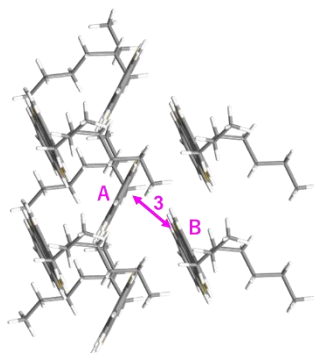
Mol A–Mol B	$E_{\text{elst}}^{\text{b}}$	$E_{\text{exch}}^{\text{b}}$	$E_{\text{indAB}}^{\text{b}}$	$E_{\text{indBA}}^{\text{b}}$	$E_{\text{disp}}^{\text{b}}$	$E_{\text{total}}^{\text{b}}$
DNTT–DNTT	-7.061	16.127	-0.748	-1.295	-23.091	-16.068
DNTT–EH	0.026	0.328	0.131	-0.021	-0.901	-0.437
EH–DNTT	-0.565	0.752	-0.041	0.021	-1.811	-1.645
EH–EH	0.012	-0.000	0.001	-0.000	-0.001	0.011
total	-7.589	17.208	-0.658	-1.295	-25.805	-18.138
SAPT0 ^c	-7.589	17.208	-0.658	-1.295	-25.805	-18.139



^a Refer the inserted figure in Table 3 for the definition of the molecular pair. ^b E_{elst} : electrostatic interaction energy, E_{exch} : exchange interaction energy, E_{indAB} : induction interaction energy, E_{indBA} : induction interaction energy, E_{disp} : dispersion energy, E_{total} : the sum of each energetic terms. ^c E_{int} separately calculated by SAPT0.

Table S3. Partitioned intermolecular interaction energy ($E_{\text{ints}} / \text{kcal mol}^{-1}$) of the molecular pair #3^a.

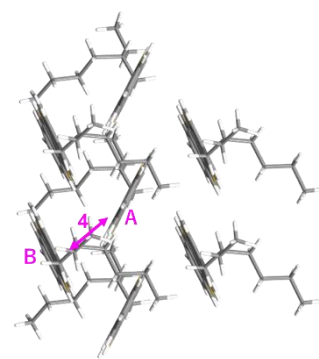
Mol A–Mol B	$E_{\text{elst}}^{\text{b}}$	$E_{\text{exch}}^{\text{b}}$	$E_{\text{indAB}}^{\text{b}}$	$E_{\text{indBA}}^{\text{b}}$	$E_{\text{disp}}^{\text{b}}$	$E_{\text{total}}^{\text{b}}$
DNTT–DNTT	-6.292	15.547	-1.248	-0.623	-22.528	-15.145
DNTT–EH	-0.344	0.007	-0.013	-0.01	-0.428	-0.789
EH–DNTT	-0.232	0.284	-0.039	0.114	-0.943	-0.816
EH–EH	0.019	-0.000	-0.001	0.001	-0.001	0.018
total	-6.849	15.838	-1.301	-0.519	-23.901	-16.732
SAPT0 ^c	-6.849	15.838	-1.301	-0.519	-23.901	-16.731



^a Refer the inserted figure in Table 3 for the definition of the molecular pair. ^b E_{elst} : electrostatic interaction energy, E_{exch} : exchange interaction energy, E_{indAB} : induction interaction energy, E_{indBA} : induction interaction energy, E_{disp} : dispersion energy, E_{total} : the sum of each energetic terms. ^c E_{int} separately calculated by SAPT0.

Table S4. Partitioned intermolecular interaction energy ($E_{\text{intS}} / \text{kcal mol}^{-1}$) of the molecular pair #4^a.

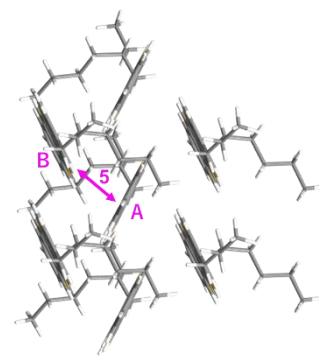
Mol A–Mol B	$E_{\text{elst}}^{\text{b}}$	$E_{\text{exch}}^{\text{b}}$	$E_{\text{indAB}}^{\text{b}}$	$E_{\text{indBA}}^{\text{b}}$	$E_{\text{disp}}^{\text{b}}$	$E_{\text{total}}^{\text{b}}$
DNTT–DNTT	-7.100	15.535	-0.656	-1.151	-21.893	-15.266
DNTT–EH	-0.162	0.839	0.060	-0.055	-1.677	-0.995
EH–DNTT	-0.350	0.284	-0.027	-0.012	-1.152	-1.257
EH–EH	0.017	-0.000	-0.000	-0.001	-0.001	0.015
total	-7.596	16.658	-0.623	-1.219	-24.722	-17.502
SAPT0 ^c	-7.596	16.659	-0.623	-1.219	-24.722	-17.502



^a Refer the inserted figure in Table 3 for the definition of the molecular pair. ^b E_{elst} : electrostatic interaction energy, E_{exch} : exchange interaction energy, E_{indAB} : induction interaction energy, E_{indBA} : induction interaction energy, E_{disp} : dispersion energy, E_{total} : the sum of each energetic terms. ^c E_{int} separately calculated by SAPT0.

Table S5. Partitioned intermolecular interaction energy ($E_{\text{intS}} / \text{kcal mol}^{-1}$) of the molecular pair #5^a.

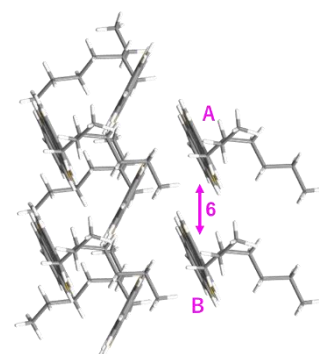
Mol A–Mol B	$E_{\text{elst}}^{\text{b}}$	$E_{\text{exch}}^{\text{b}}$	$E_{\text{indAB}}^{\text{b}}$	$E_{\text{indBA}}^{\text{b}}$	$E_{\text{disp}}^{\text{b}}$	$E_{\text{total}}^{\text{b}}$
DNTT–DNTT	-5.904	14.252	-1.209	-0.536	-21.520	-14.917
DNTT–EH	-0.375	0.832	0.001	-0.066	-1.976	-1.585
EH–DNTT	-0.230	1.285	-0.072	0.040	-2.031	-1.010
EH–EH	0.011	-0.000	-0.001	-0.001	-0.001	0.009
total	-6.498	16.369	-1.282	-0.563	-25.528	-17.502
SAPT0 ^c	-6.498	16.369	-1.282	-0.563	-25.528	-17.502



^a Refer the inserted figure in Table 3 for the definition of the molecular pair. ^b E_{elst} : electrostatic interaction energy, E_{exch} : exchange interaction energy, E_{indAB} : induction interaction energy, E_{indBA} : induction interaction energy, E_{disp} : dispersion energy, E_{total} : the sum of each energetic terms. ^c E_{int} separately calculated by SAPT0.

Table S6. Partitioned intermolecular interaction energy ($E_{\text{intS}} / \text{kcal mol}^{-1}$) of the molecular pair #6^a.

Mol A–Mol B	$E_{\text{elst}}^{\text{b}}$	$E_{\text{exch}}^{\text{b}}$	$E_{\text{indAB}}^{\text{b}}$	$E_{\text{indBA}}^{\text{b}}$	$E_{\text{disp}}^{\text{b}}$	$E_{\text{total}}^{\text{b}}$
DNTT–DNTT	-7.793	14.026	-0.843	-0.843	-15.530	-10.983
DNTT–EH	-0.336	0.008	0.024	-0.019	-0.364	-0.687
EH–DNTT	-0.109	0.007	-0.031	-0.003	-0.436	-0.573
EH–EH	0.013	0.385	0.007	-0.005	-1.692	-1.292
total	-8.226	14.426	-0.843	-0.870	-18.021	-13.534
SAPT0 ^c	-8.226	14.426	-0.843	-0.870	-18.021	-13.534



^a Refer the inserted figure in Table 3 for the definition of the molecular pair. ^b E_{elst} : electrostatic interaction energy, E_{exch} : exchange interaction energy, E_{indAB} : induction interaction energy, E_{indBA} : induction interaction energy, E_{disp} : dispersion energy, E_{total} : the sum of each energetic terms. ^c E_{int} separately calculated by SAPT0.

15. XRD curves of EH-BTBTs spin-coated thin films

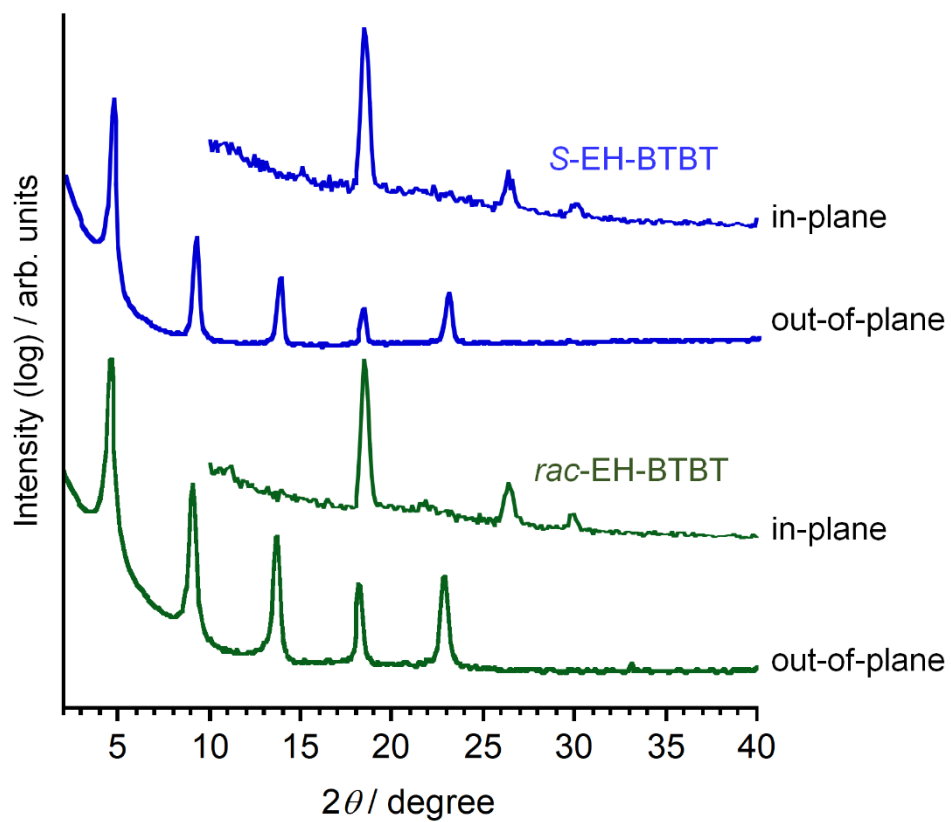


Fig. S15. Out-of-plane and in-plane XRD patterns of spin-coated thin film of *S*-EH-BTBT (blue) and *rac*-EH-BTBT (green) on OTS-treated SiO₂/Si substrates

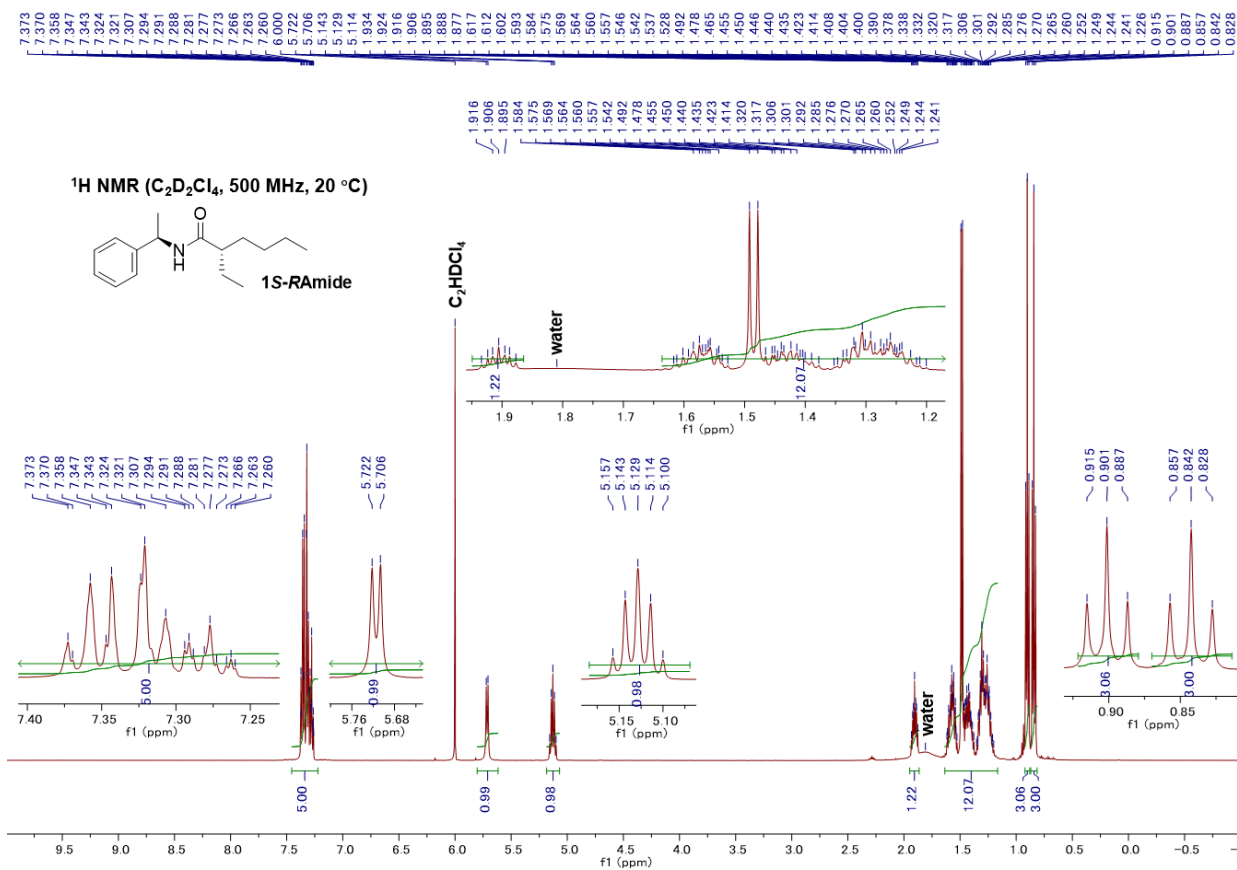


Fig. S18. ¹H NMR spectrum of **1R-Samide**.

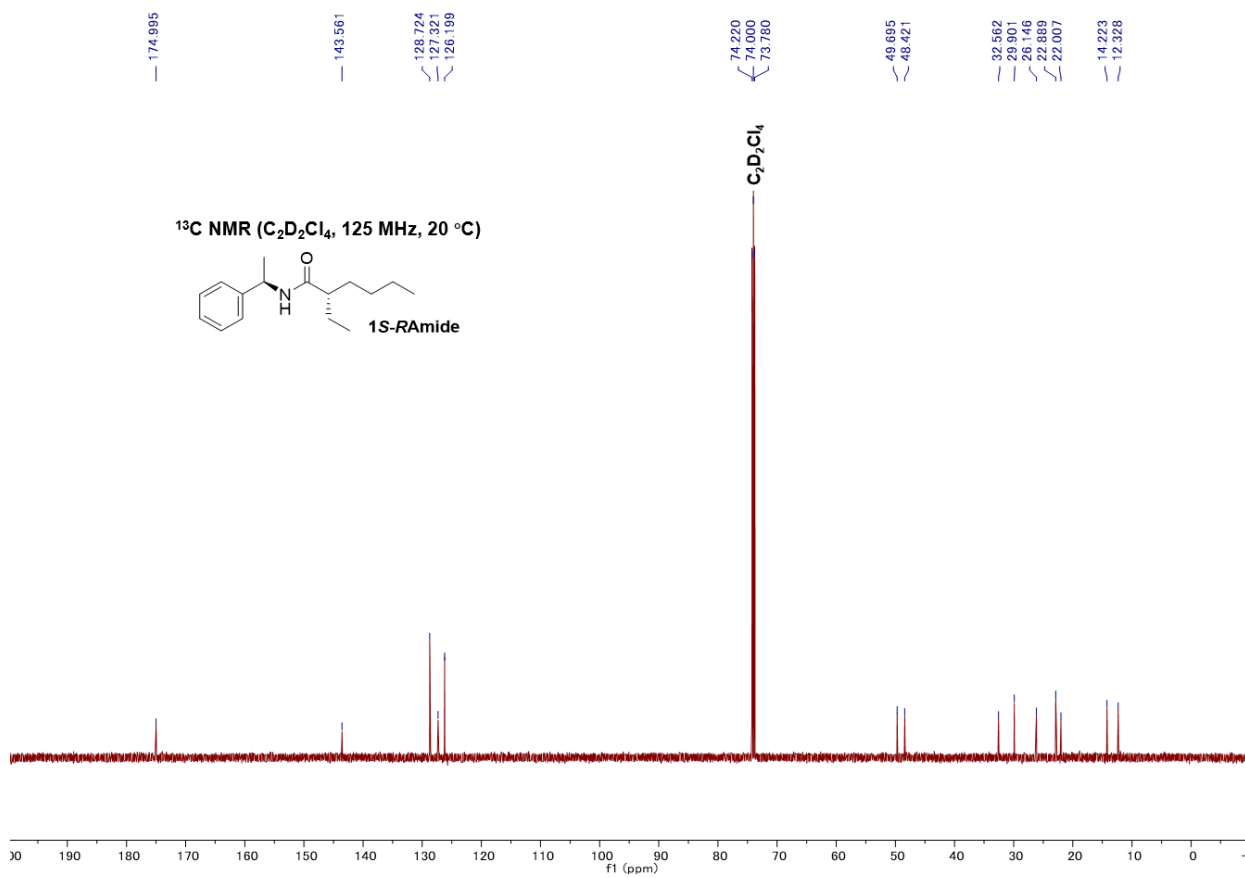


Fig. S19. ¹³C NMR spectrum of **1R-Samide**.

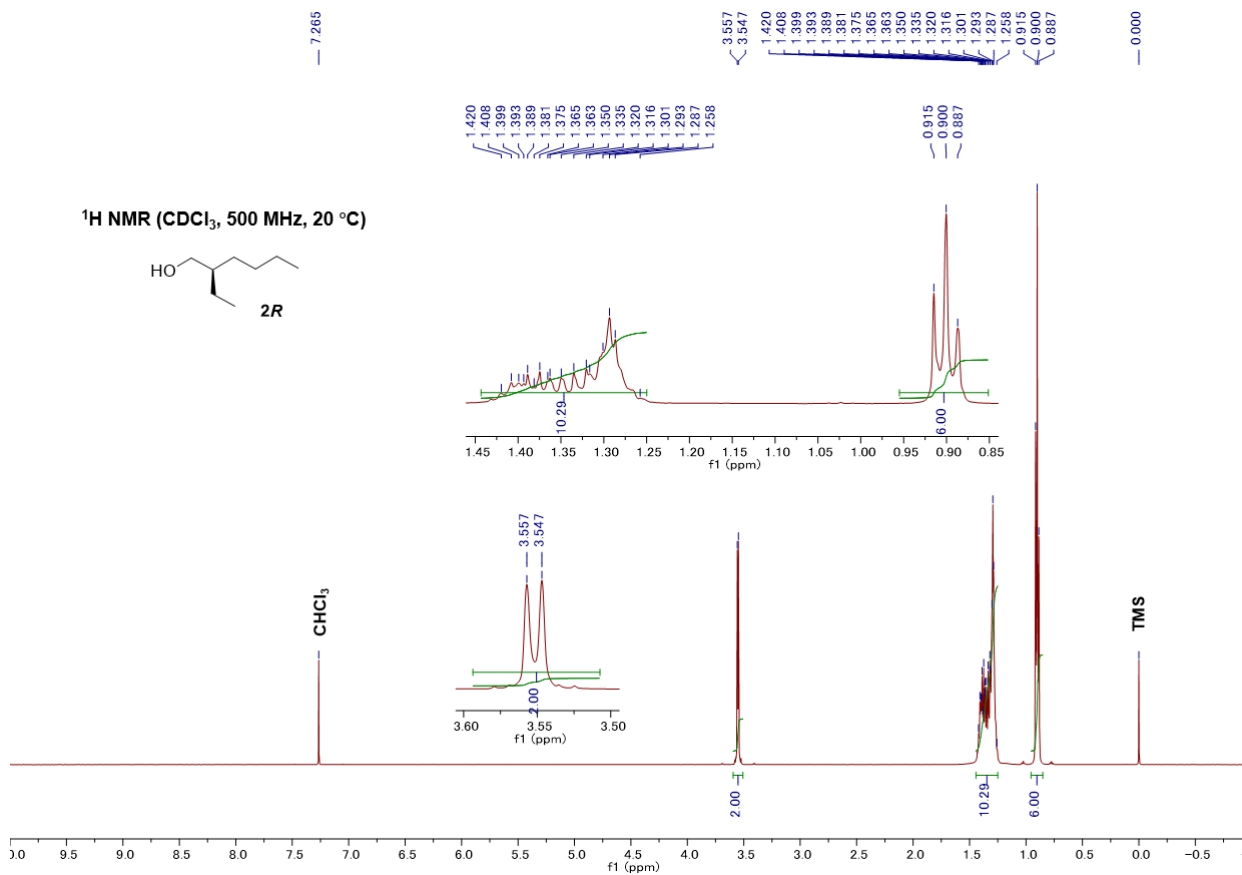


Fig. S20. ¹H NMR spectrum of **2R**.

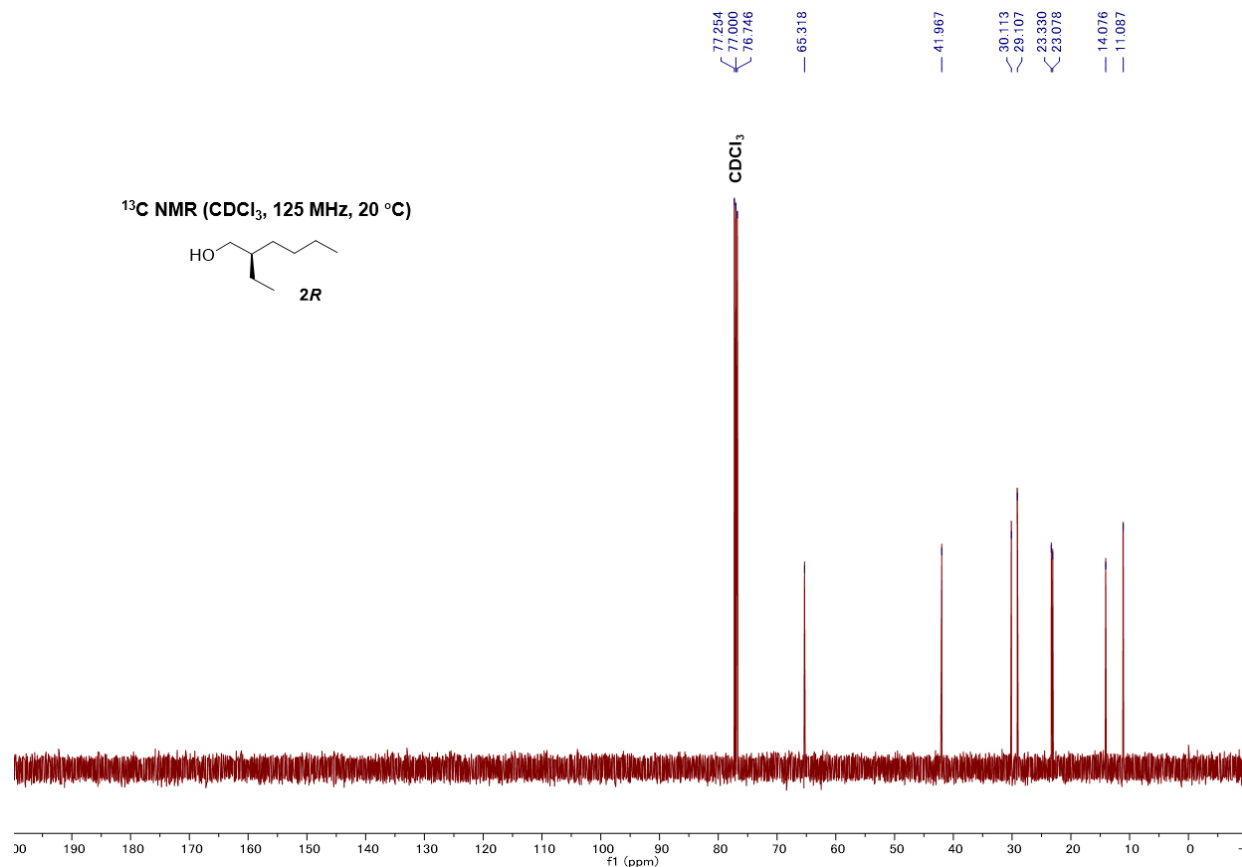


Fig. S21. ¹³C NMR spectrum of **2R**.

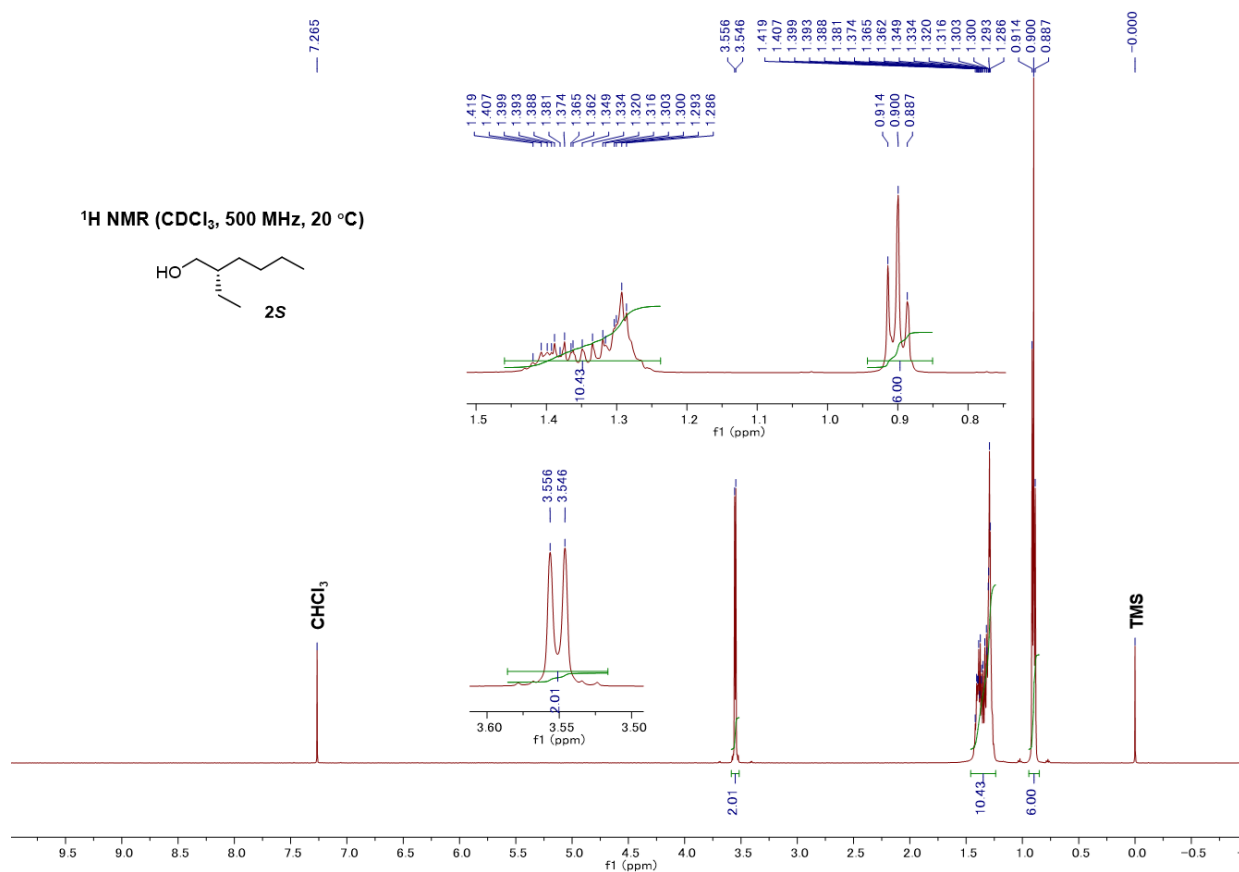


Fig. S22. ¹H NMR spectrum of **2S**.

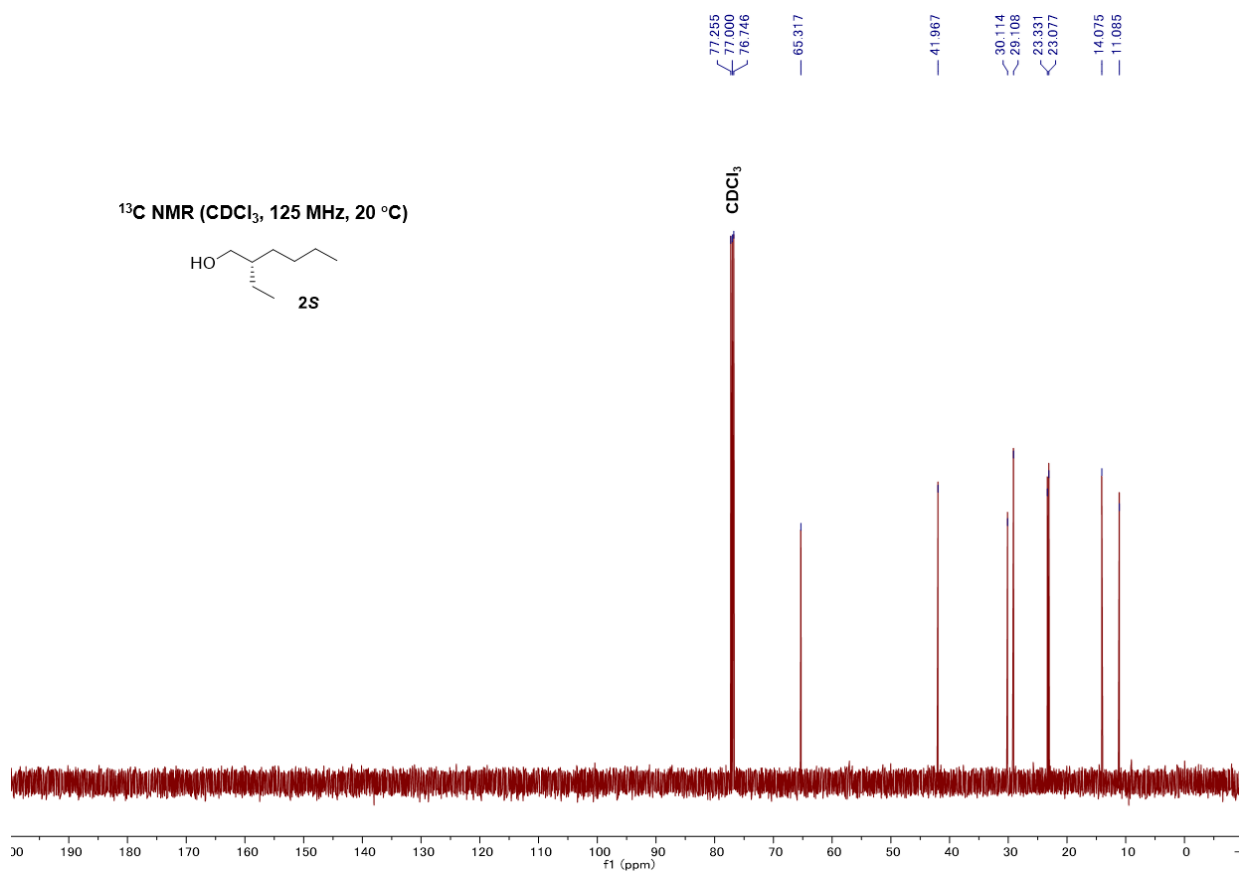


Fig. S23. ¹³C NMR spectrum of **2S**.

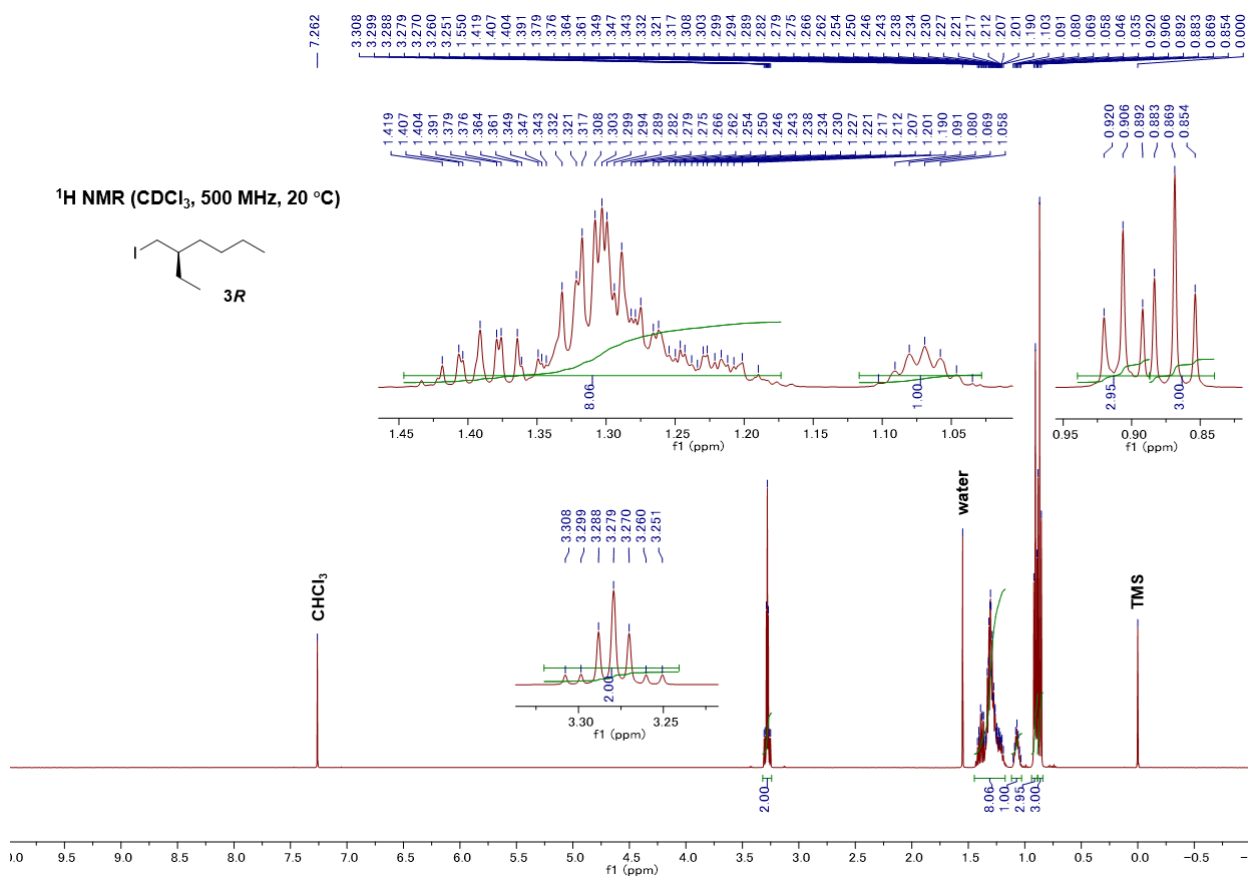


Fig. S24. ¹H NMR spectrum of **3R**.

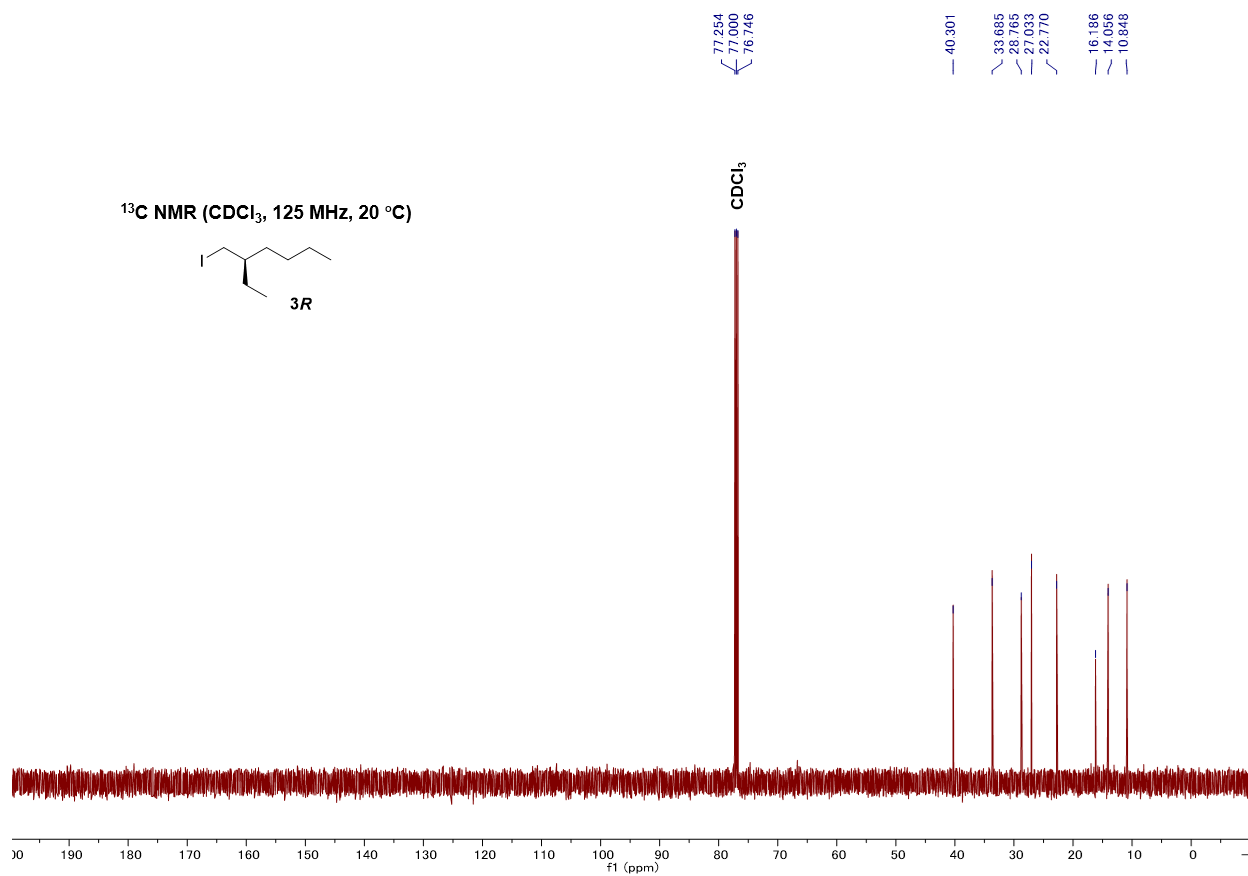


Fig. S25. ¹³C NMR spectrum of **3R**.

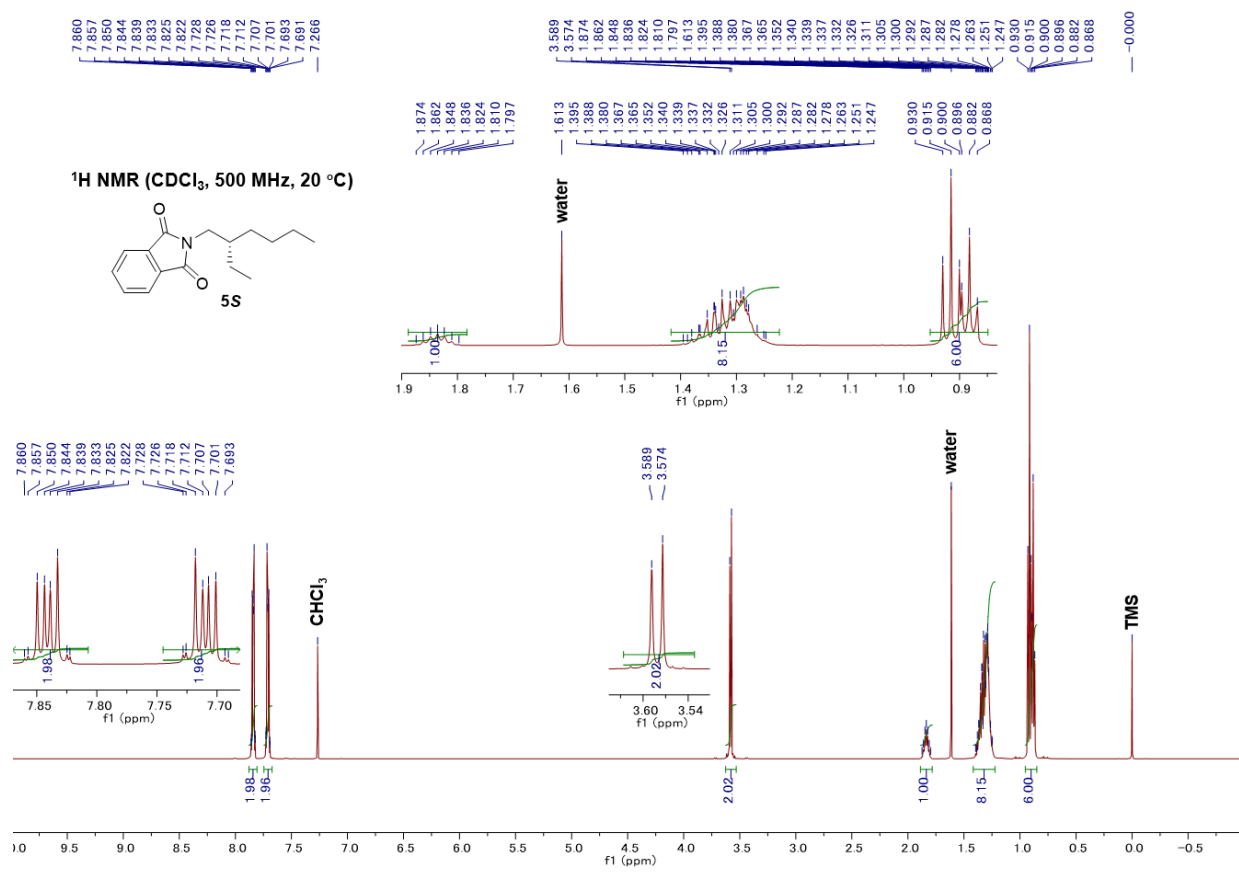


Fig. S38. ¹H NMR spectrum of **5S**.

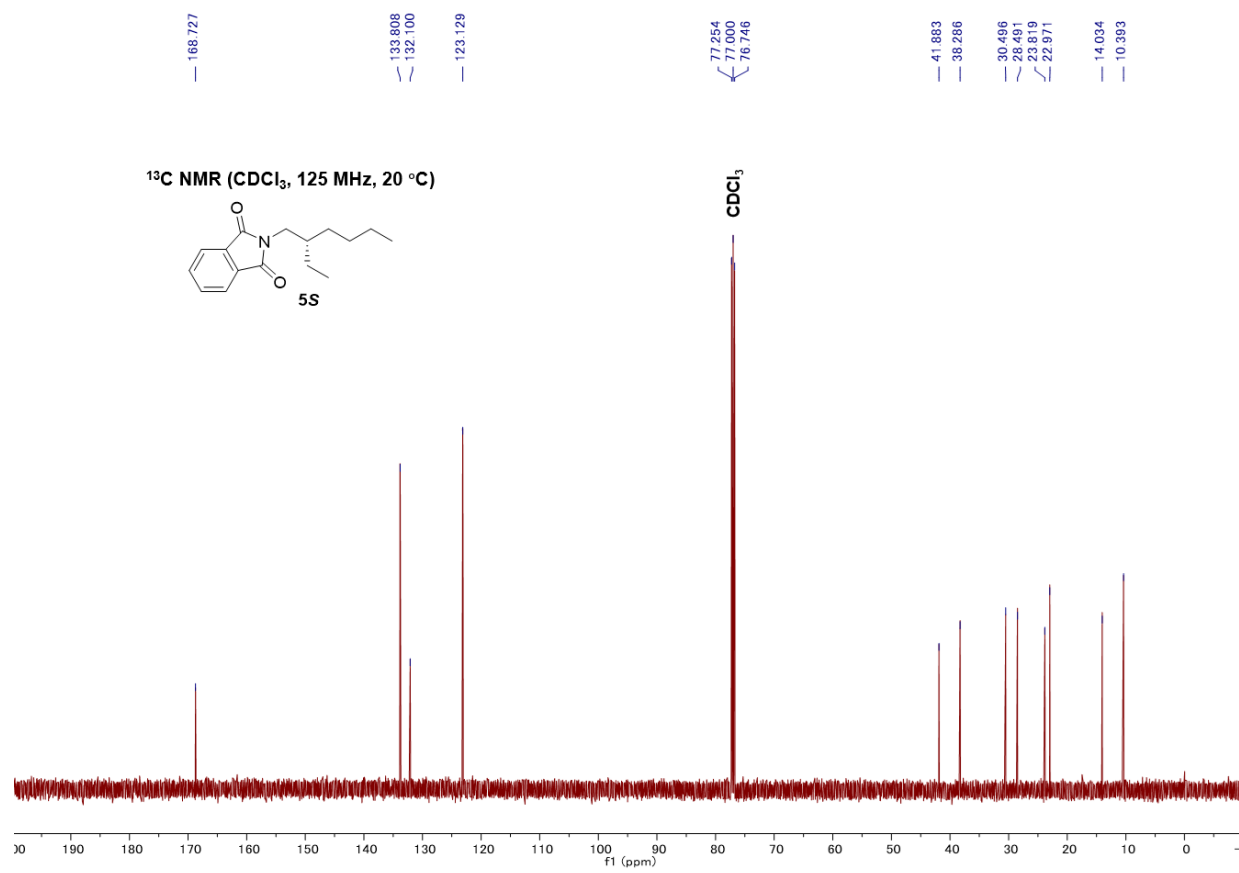


Fig. S39. ¹³C NMR spectrum of **5S**.

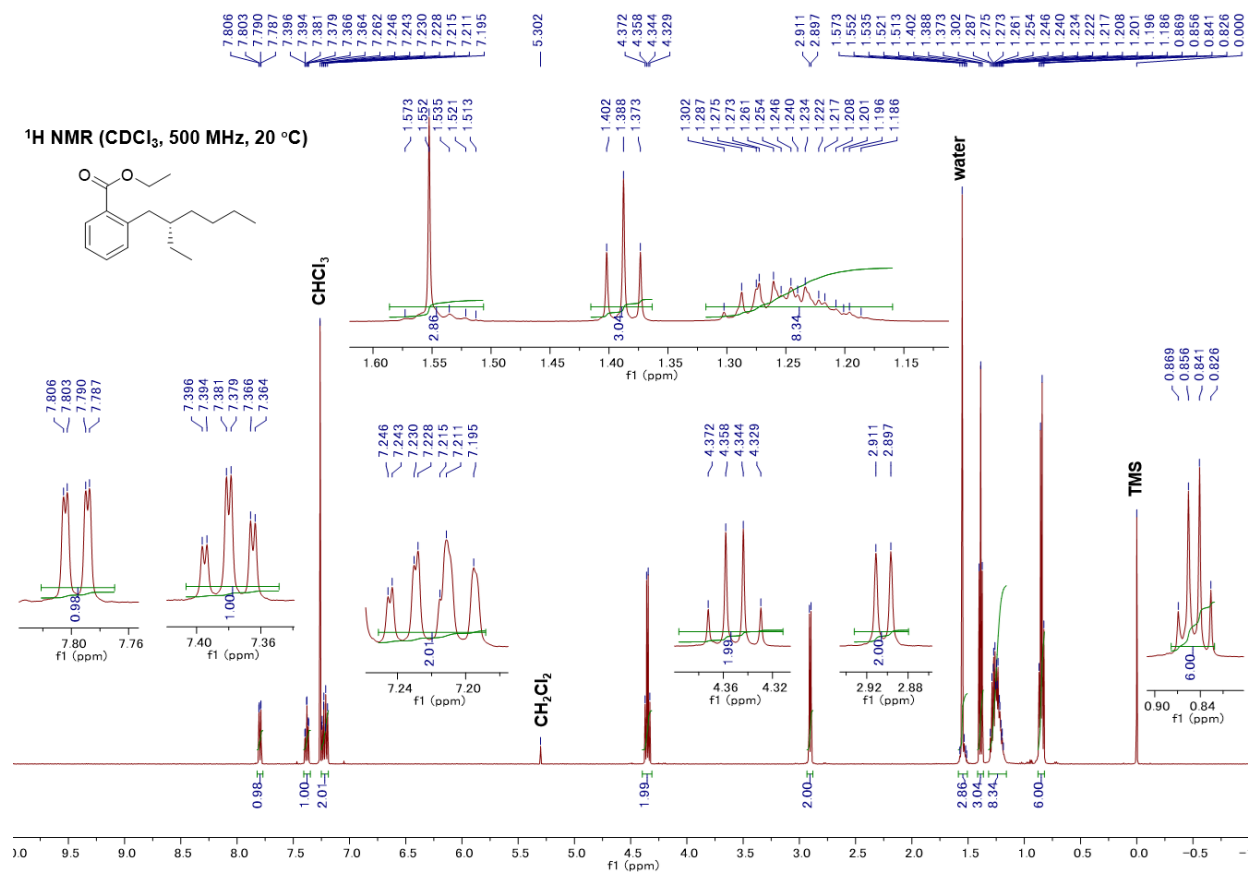


Fig. S42. ¹H NMR spectrum of **6S**.

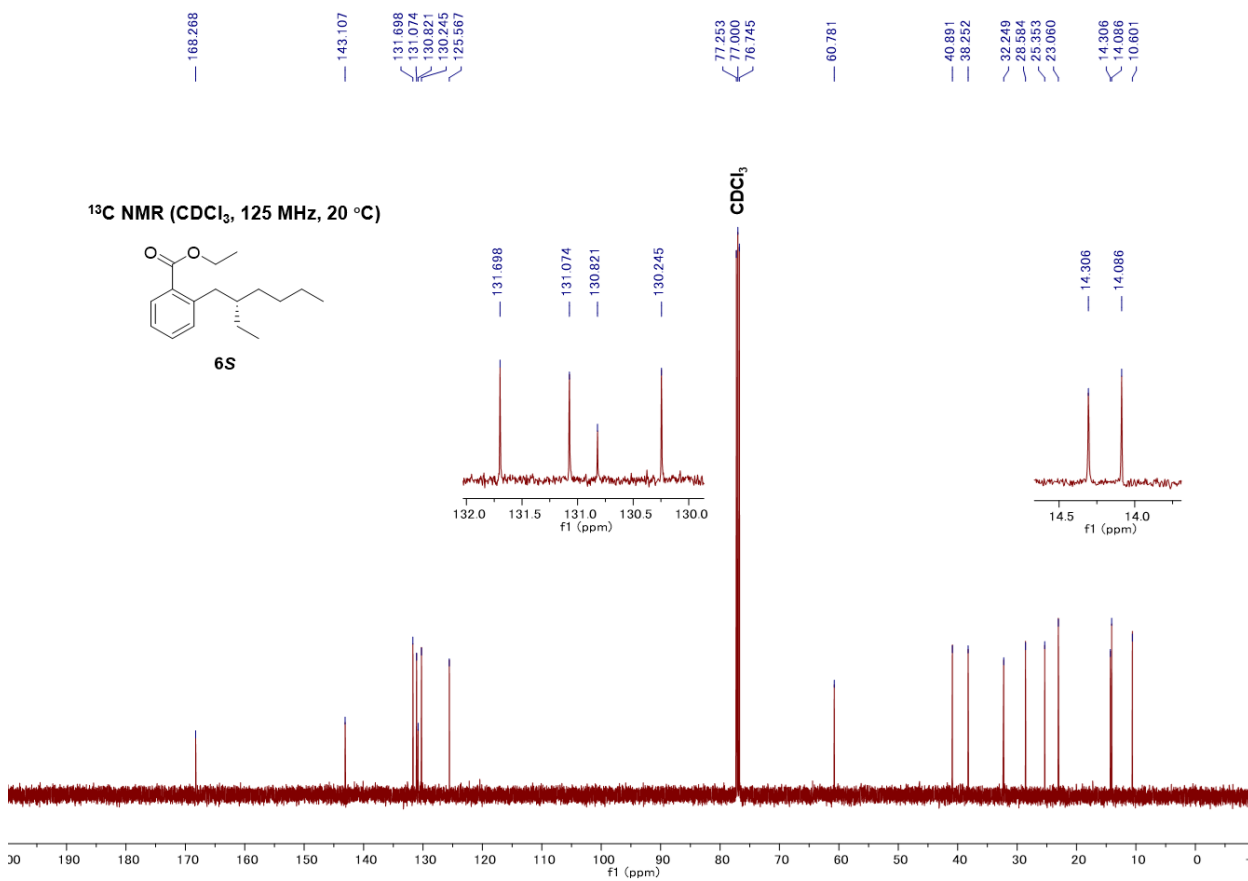


Fig. S43. ¹³C NMR spectrum of **6S**.

17. References

- S1. K. Kawabata, S. Usui and K. Takimiya, *J. Org. Chem.*, 2020, **85**, 195-206.
- S2. E. Pump, A. Poater, M. Zirngast, A. Torvisco, R. Fischer, L. Cavallo and C. Slugovc, *Organometallics*, 2014, **33**, 2806-2813.
- S3. S. Inoue, H. Minemawari, J. y. Tsutsumi, M. Chikamatsu, T. Yamada, S. Horiuchi, M. Tanaka, R. Kumai, M. Yoneya and T. Hasegawa, *Chem. Mater.*, 2015, **27**, 3809-3812.
- S4. M. J. Frisch, G. W. Trucks, H. B. Schlegel, G. E. Scuseria, M. A. Robb, J. R. Cheeseman, G. Scalmani, V. Barone, G. A. Petersson, H. Nakatsuji, X. Li, M. Caricato, A. V. Marenich, J. Bloino, B. G. Janesko, R. Gomperts, B. Mennucci, H. P. Hratchian, J. V. Ortiz, A. F. Izmaylov, J. L. Sonnenberg, Williams, F. Ding, F. Lipparini, F. Egidi, J. Goings, B. Peng, A. Petrone, T. Henderson, D. Ranasinghe, V. G. Zakrzewski, J. Gao, N. Rega, G. Zheng, W. Liang, M. Hada, M. Ehara, K. Toyota, R. Fukuda, J. Hasegawa, M. Ishida, T. Nakajima, Y. Honda, O. Kitao, H. Nakai, T. Vreven, K. Throssell, J. A. Montgomery Jr., J. E. Peralta, F. Ogliaro, M. J. Bearpark, J. J. Heyd, E. N. Brothers, K. N. Kudin, V. N. Staroverov, T. A. Keith, R. Kobayashi, J. Normand, K. Raghavachari, A. P. Rendell, J. C. Burant, S. S. Iyengar, J. Tomasi, M. Cossi, J. M. Millam, M. Klene, C. Adamo, R. Cammi, J. W. Ochterski, R. L. Martin, K. Morokuma, O. Farkas, J. B. Foresman and D. J. Fox, *Journal*, 2016, Gaussian 16 Rev. C.01.
- S5. R. M. Parrish, L. A. Burns, D. G. A. Smith, A. C. Simmonett, A. E. DePrince, E. G. Hohenstein, U. Bozkaya, A. Y. Sokolov, R. Di Remigio, R. M. Richard, J. F. Gonthier, A. M. James, H. R. McAlexander, A. Kumar, M. Saitow, X. Wang, B. P. Pritchard, P. Verma, H. F. Schaefer, K. Patkowski, R. A. King, E. F. Valeev, F. A. Evangelista, J. M. Turney, T. D. Crawford and C. D. Sherrill, *J. Chem. Theory Comput.*, 2017, **13**, 3185-3197.
- S6. R. M. Parrish, T. M. Parker and C. D. Sherrill, *J. Chem. Theory Comput.*, 2014, **10**, 4417-4431.
- S7. ADF: powerful DFT code for modeling molecules; Scientific Computing and Modeling: Amsterdam; <http://www.scm.com/ADF/>).
- S8. Z. Xu, Y. Zhang, H. Fu, H. Zhong, K. Hong and W. Zhu, *Bioorg. Med. Chem. Lett.*, 2011, **21**, 4005-4007.
- S9. J. V. B. Kanth and M. Periasamy, *J. Org. Chem.*, 1991, **56**, 5964-5965.
- S10. L. Jones, J. S. Schumm and J. M. Tour, *J. Org. Chem.*, 1997, **62**, 1388-1410.
- S11. C. Gröst, M. Gräber, M. Hell and T. Berg, *Bioorg. Med. Chem.*, 2013, **21**, 7357-7363.
- S12. G. Sheldrick, *Acta Crystallogr. Sec. A*, 2015, **71**, 3-8.
- S13. G. Sheldrick, *Acta Crystallogr. Sec. C*, 2015, **71**, 3-8.
- S14. O. V. Dolomanov, L. J. Bourhis, R. J. Gildea, J. A. K. Howard and H. Puschmann, *J. Appl. Crystallogr.*, 2009, **42**, 339-341.